Geochimica et Cosmochimica Acta 369 (2024) 179–195

Contents lists available at ScienceDirect

Geochimica et Cosmochimica Acta

journal homepage: www.elsevier.com/locate/gca

A carbon, nitrogen, and multi-isotope study of basalt glasses near 14°N on the Mid-Atlantic Ridge. Part B: Mantle source heterogeneities

D.V. Bekaert [a,b,*], P.H. Barry [a], J. Curtice [a], J. Blusztajn [c], M. Hudak [a], A. Seltzer [a], M.W. Broadley [a], J.A. Krantz [a], V.D. Wanless [d], S.A. Soule [e], E. Mittelstaedt [f], M.D. Kurz [a]

[a] Marine Chemistry and Geochemistry Department, WHOI, Woods Hole, MA, USA
[b] Centre de Recherches Pétrographiques et Géochimiques, Vandoeuvre-lès-Nancy, France
[c] Geology and Geophysics Department, WHOI, Woods Hole, MA, USA
[d] Department of Geosciences, Boise State University, 83725 Boise, ID, USA
[e] Marine Geology and Geophysics Department, The University of Rhode Island, MA, USA
[f] Department of Earth and Spatial Sciences, University of Idaho, 83844 Moscow, ID, USA

ARTICLE INFO

Associate editor: Manuel Moreira

Keywords:
Popping rocks
Mantle source heterogeneities
Subduction-driven recycling
Primordial volatiles
HIMU
Oceanic Core Complexes
Mantle carbon
Mantle nitrogen
Planetary evolution

ABSTRACT

Geochemical variations along mid-ocean ridges reveal the heterogeneous nature of the convecting upper mantle and geodynamic evolution of our planet (e.g., Hofmann, 2007; Parai et al., 2012). Although the occurrence of incompatible element and isotopically enriched mid-ocean ridge basalts (E-MORB) commonly arises from interaction with nearby mantle plumes, the source of E-MORBs far from known hotspots is debated. A well-known example of an enigmatic geochemical enrichment is found at 14°N on the Mid-Atlantic ridge (MAR). This is also one of the few locations worldwide where volatile-saturated E-MORBs, often referred to as "popping rocks" (PR), have been recovered. Although the mechanism(s) involved in popping rock generation remain elusive, compressional regimes associated with the exhumation and formation of oceanic core complexes (OCC) may be required to produce popping rocks via protracted volatile accumulation. However, the geochemical signature of OCC samples and their potential relationship to local geochemical enrichments associated with popping rock-affiliated MORBs remain unknown. Here, we present a comprehensive volatile characterization of popping rocks and associated MORBs (n = 19) sampled at 14°N on the MAR, including (n = 2) normal MORBs (N-MORB) from an oceanic core complex (OCC) and (n = 17) E-MORBs (Bekaert et al., Part A). We use isotopic and abundance data for volatile (carbon, nitrogen, noble gases) and radiogenic (Pb, Sr, Nd) elements, as well as the abundances of major and trace elements, to elucidate on the source(s) of E-MORBs at 14°N and discuss the potential origin(s) of geochemical heterogeneities within the upper mantle. We observe co-variations of helium and radiogenic element isotopes, suggesting potential contributions from a young HIMU-type (high μ = time-integrated $^{238}U/^{204}Pb$) component in the OCC mantle source. The mantle source of the OCC samples is clearly distinct from that of PR-affiliated samples, suggesting no genetic relationship between OCC samples and E-MORBs. In addition, elevated Dy/Yb in OCC samples likely point to the incorporation of a subducted crustal component that is not observed in the mantle source of other MORB samples analyzed in this study. We report mantle source $^{40}Ar/^{36}Ar$ variations at 14°N, which, in line with previous studies, are interpreted as primarily reflecting variations in the amounts of recycled atmospheric Ar. Despite extensive evidence for drastic geochemical heterogeneities at 14°N on the MAR, we observe no significant $\delta^{15}N$ variation (average $\delta^{15}N = -4.49 \pm 1.40$ ‰) across N-MORB and E-MORB samples. This is a fundamental constraint, as the absence of significant N isotope variations across the upper mantle may imply that sedimentary N (with a typical $\delta^{15}N \sim +6$‰) is not extensively introduced within this reservoir during subduction. We investigate several scenarios that could explain this observation, including a significant contribution of altered oceanic crust to the overall budget of subducting slabs, quantitative return of subducting sedimentary N to the Earth's surface by arc volcanism, and/or preferential transport/preservation of sedimentary N in the lower mantle source of oceanic island basalts.

* Corresponding author.
E-mail address: david.bekaert@univ-lorraine.fr (D.V. Bekaert).

https://doi.org/10.1016/j.gca.2023.12.017
Received 23 October 2023; Accepted 14 December 2023
Available online 20 December 2023

1. Introduction

From a major/trace element and radiogenic isotope perspective, the MORB mantle appears geochemically heterogeneous on local (sub-kilometer) through global (ocean basin) scales (e.g., Bougault et al., 1988; Schilling et al., 1994; Hofmann, 2007). While the major element and petrological properties of MORB provide insight into the melting processes occurring beneath ridges (e.g., Klein and Langmuir, 1987), the range of basaltic isotopic compositions and geochemical variability provide information about mantle source features. For example, geochemically-enriched basalts (E-MORB), with elevated concentrations of K_2O and other highly incompatible elements, are less abundant than normal (N-type) MORB. The extent and origin of geochemical heterogeneities observed along mid-ocean ridges has remained a subject of great debate (e.g., Donnelly et al., 2004; Hofmann, 2007; Meyzen et al., 2007; Liu and Liang, 2017), potentially involving contributions from (i) recycled material (e.g., oceanic crust, alkali basalts from seamounts), (ii) mantle plume-derived material, and/or (iii) metasomatic enrichments of the lower oceanic crust by infiltration of low-degree melts (e.g., Allègre and Turcotte, 1986; Donnelly et al., 2004; Stracke, 2012; Ulrich et al., 2012).

Part of the geochemical variability observed within the solid Earth could also reflect primordial heterogeneities that have not been evenly distributed by convective mixing. For example, mantle plumes tapping into the deepest portions of Earth's mantle show evidence for the preservation of primordial signatures that were inherited from the early stages of terrestrial formation and differentiation (e.g., Mukhopadhyay, 2012; Mundl-Petermeier et al., 2020; Broadley et al., 2020). The lateral entrainment and dispersal of "blobs" or veins of plume material throughout the convecting mantle has the potential to scatter enriched geochemical signatures far from plume conduits rooted in the deep Earth (Allègre et al., 1984; Koppers et al., 2021). The motion of these so-called blobs may either be driven by physical interaction with the asthenospheric mantle flow field or by pressure gradients at sub-lithospheric depths (e.g., Sleep, 1996; Bekaert et al., 2021a). In addition, the protracted injection of oceanic lithosphere into the mantle during subduction has introduced differentiated and geochemically-enriched material into the solid Earth for up to 3 billion years (e.g., Anderson, 2006; Shirey and Richardson, 2011; Smit et al., 2019). However, the relative contributions of these different processes, and their roles in generating a heterogeneous upper mantle, remains under-constrained.

We present and discuss a comprehensive set of volatile (C, N, He, Ne, Ar) and radiogenic element (Pb, Sr, Nd) isotopes, as well as major and trace element data for a suite of (n = 19) seafloor basaltic glasses from different tectonic settings, collected between 2016 and 2018 near 14°N on the MAR using R/V Atlantis and the human occupied submarine vehicle Alvin (Péron et al., 2019; Jones et al., 2019; Parnell-Turner et al., 2018). The sample set consists of (n = 5) popping rocks (hereafter "PR"), (n = 6) low-vesicularity (<3 vol%) MORBs with PR-like trace element patterns ("PRTE-LV"), (n = 6) non-popping rocks ("NPR"), and (n = 2) MORBs recovered from an oceanic core complex ("OCC"), located off-axis of the MAR (Parnell-Turner et al., 2018). This extensive dataset is used in combination with data reported in Bekaert *et al.*, **Part A** to provide novel insights into the extent and origin of geochemical heterogeneities at 14°N on the MAR and, more generally, across the upper mantle. The paper is basically structured as follows: first, major and trace element, radiogenic isotope, and noble gas isotope data are considered together in order to investigate potential sources of observed mantle source heterogeneities (i.e., occurrence of plume-derived and recycled (crustal and/or sedimentary) components. These signatures are then tentatively related to observed mantle source C/^{3}He, C/N, and N_2/^{3}He variations. A special focus is set on the remarkable – but puzzling – N isotope homogeneity of the upper mantle, which appears at odds with the widespread occurrence of surface-derived, recycled components with presumably distinct N isotope compositions.

2. Methods

2.1. Pb-Sr-Nd isotope analyses

For each sample, >200 mg of fresh glass chips was first acid leached in 6.2 N HCl for 1 h at 100 °C. HCl was then pipetted off and the samples were rinsed twice in Milli-Q H_2O. For Sr, Nd and Pb, separation-leached samples were dissolved in a 3:1 mixture of concentrated HF: HNO_3, followed by three dry downs in 6.2 N HCl to convert fluorides to chlorides. Lead was separated following the HBr-HNO_3 procedure of Abouchami et al. (1999) using a single column pass. Separation of Sr and Nd was carried out with Eichrom Sr-Spec and Ln-Spec resin, respectively. Sr and Nd were recovered from the clean wash of the Pb columns. This wash fraction was split in two, one destined for the Sr separation protocol and the other destined for the Nd separation protocol. In this manner, Pb, Nd, and Sr were all separated from the same sample dissolutions, thereby avoiding potential problems due to possible sample heterogeneity.

The total procedural blanks for Pb, Sr and Nd were < 30 pg, < 80 pg and < 35 pg, respectively, which are all negligible relative to the amount of Sr, Nd and Pb analyzed in the rocks. All Pb, Sr and Nd isotopic measurements were performed on the Neptune MC-ICP-MS at Woods Hole Oceanographic Institution (WHOI). The well-characterized USGS standard BHVO-1 was measured with results for Sr, Nd and Pb isotopic compositions of $^{87}Sr/^{86}Sr$ = 0.703466, $^{143}Nd/^{144}Nd$ = 0.51298, $^{206}Pb/^{204}Pb$ = 18.689, $^{207}Pb/^{204}Pb$ = 15.567, $^{208}Pb/^{204}Pb$ = 38.339. After renormalization based on (Abouchami et al., 2000), the Pb isotopic results are $^{206}Pb/^{204}Pb$ = 18.694, $^{207}Pb/^{204}Pb$ = 15.574, $^{208}Pb/^{204}Pb$ = 38.361, which are within error of former work (Weis et al., 2006).

2.1.1. Lead isotope analysis

Lead isotopic ratios were corrected for instrumental mass bias by introducing Tl (SRM 997) as an internal standard to sample Pb solutions prior to each run, assuming a $^{205}Tl/^{203}Tl$ ratio of 2.38709. Mass 202 was monitored to correct for ^{204}Hg interference, but this correction was small owing to low $^{202}Hg/^{208}Pb$ ratios (typically < $1.0x10^{-5}$). Measured Pb-isotopic ratios of the samples were normalized based on the offset between our average measured and the accepted SRM981 values from (Todt et al., 1996) ($^{206}Pb/^{204}Pb$ = 16.9356, $^{207}Pb/^{204}Pb$ = 15.4891, $^{208}Pb/^{204}Pb$ = 36.7006). External reproducibility on runs of SRM981 at WHOI ranges from 17 ppm (2σ) for $^{207}Pb/^{206}Pb$ to 117 ppm (2σ) for $^{208}Pb/^{204}Pb$ (Hart et al., 2004).

2.1.2. Strontium isotope analysis

During each analytical session, intensities were measured on masses 82 through 88. Corrections for isobaric interferences of Rb on mass 87 and Kr on masses 84 and 86 were made offline following the procedures outlined in Jackson and Hart (2006). Strontium isotope ratios were corrected for instrumental mass bias relative to an $^{86}Sr/^{88}Sr$ value of 0.1194. $^{87}Sr/^{86}Sr$ ratios for unknowns were then normalized by the offset between our average measured value of SRM987 during each analytical session and the accepted $^{87}Sr/^{86}Sr$ of 0.710240 (Jackson and Hart, 2006). The external precision of the $^{87}Sr/^{86}Sr$ measurements is estimated to be 15–25 ppm (2σ) (Hart and Blusztajn, 2006).

2.1.3. Neodymium isotope analysis

The data were corrected for instrumental mass fractionation relative to a $^{146}Nd/^{144}Nd$ value of 0.7219. Both the La Jolla and JNdi-1 standards were run during each analytical session. The $^{143}Nd/^{144}Nd$ values for JNdi-1 were adapted to the La Jolla $^{143}Nd/^{144}Nd$ value using a ratio of 1.000503 (Tanaka et al., 2000). The La Jolla and La Jolla-renormalized-JNdi-1 $^{143}Nd/^{144}Nd$ measurements were averaged to give a final La Jolla average for each analytical session. Samples were normalized based on the offset of this La Jolla average and the actual La Jolla $^{143}Nd/^{144}Nd$ value of 0.511847 (White and Patchett, 1984). The external precision of the $^{143}Nd/^{144}Nd$ measurements is estimated to be 15–25 ppm (2σ) (Hart

and Blusztajn, 2006).

3. Results

3.1. Major and trace element data

Major and trace element data are reported in Bekaert et al., **Part A.** They demonstrate a wide range in MORB compositions, from E-MORB (PR-affiliated samples) to N-MORB (OCC samples) end-members (Fig. 1), with non-popping rock samples (NPR) spanning a wider range of chemical compositions across the T-MORB to E-MORB ranges.

3.2. Radiogenic isotope variations

Radiogenic isotope data measured in this study are reported in Table 1. The Pb, Sr, and Nd isotope variations observed among PR, PRTE-LV, NPR, and OCC samples support the existence of geochemical heterogeneities in the mantle source of MORBs near 14°N (Fig. 2). In line with major and trace element systematics, we find that PR-affiliated and OCC samples represent the two most extreme mantle source end-members in radiogenic isotope space. In particular, OCC samples exhibit a distinct signature of lower $^{143}Nd/^{144}Nd$ and $^{87}Sr/^{86}Sr$ and more radiogenic Pb isotopes than the mantle source of PR-affiliated samples (Fig. 2). Akin to major and trace element systematics (Bekaert et al., **Part A**), NPR samples show more isotopic variability, spanning the entire compositional range between PR-affiliated and OCC end-members.

3.3. Noble gas isotope variations

3.3.1. He isotope systematics

Most of the MORB samples analyzed in this study show $^{3}He/^{4}He$ values within the range of previously analyzed MORBs (i.e., 8 ± 1 times R_A, where R_A is the atmospheric $^{3}He/^{4}He$ of $1.384x10^{-6}$; Clarke et al., 1976). However, the OCC samples exhibit $^{3}He/^{4}He$ of ~6.8 R_A, lower than the typical MORB range, while PR and PRTE-LV (hereafter referred to as PR-affiliated samples) show typical $^{3}He/^{4}He$ ratios between ~7.6 and 8.5 R_A (Fig. 3). Low $^{3}He/^{4}He$ values - akin to those observed here for OCC samples - have previously been reported for many MORBs world-wide, including some originating from elsewhere on the MAR (near 37° N, down to 6.5 Ra, (Kurz et al., 1982)), from the ultra-slow spreading western Southwest Indian Ridge (SWIR, down to 6.3 R_A; Georgen et al., 2003), from the Australian-Antarctic Discordance (down to 6.2 R_A; Graham et al., 2001), and from the Galápagos Spreading Center (Colin et al., 2011). We find that the $^{3}He/^{4}He$ of NPR samples are more variable, spanning the entire range of values between PR-affiliated and OCC samples, similar to radiogenic isotope systematics. Overall, He isotope data appear to correlate with Pb, Sr, and Nd isotope data across the (n = 19) MORB samples (Fig. 3), implying that He isotope variations at 14°N directly reflect mantle source heterogeneities sampled by distinct eruptive events.

3.3.2. Ne and Ar isotope systematics

Neon isotope data for the (n = 19) MORB samples show limited, if any, deviation from the MORB line previously defined from the analysis of popping rock 2πD43 by Moreira et al. (1998) (**Figure S1**). With respect to Ar isotopes, PR and PRTE-LV samples broadly define two distinct compositions, marked by maximum $^{40}Ar/^{36}Ar$ at ~16,000 and

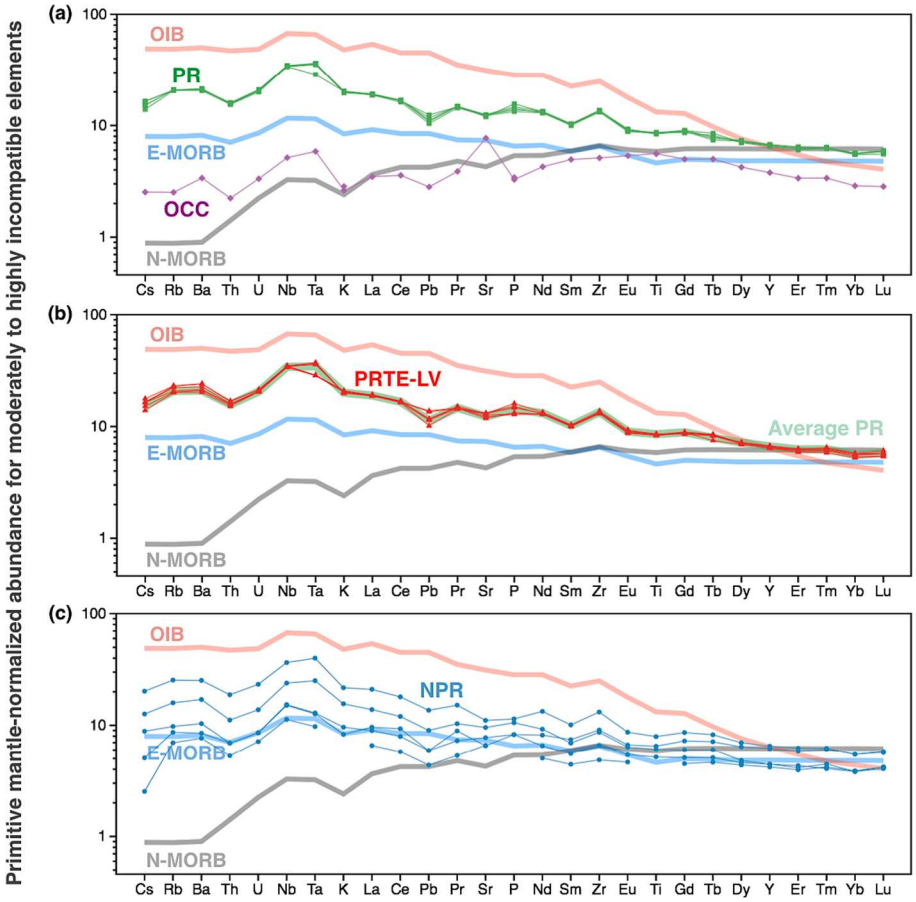

Fig. 1. Primitive mantle-normalized trace element abundance patterns for MORB samples analyzed in this study. Average N-MORB, E-MORB, oceanic alkali basalts (OIB), as well as primitive mantle values are from Sun and McDonough (1989).

Table 1
Radiogenic isotope composition of MORB samples analyzed in this study. The classification refers to popping rocks ("PR"), non-popping rocks ("NPR"), MORBs recovered from oceanic core complexes ("OCC"), and low-vesicularity (<3 vol%) MORBs with popping rock-like trace element patterns ("PRTE-LV"). NPR*: NPR sample dredged at the same latitude as OCC samples.

Sample	Classification	$^{206}Pb/^{204}Pb$	$^{207}Pb/^{204}Pb$	$^{208}Pb/^{204}Pb$	$^{87}Sr/^{86}Sr$	$^{143}Nd/^{144}Nd$
AL4818-003	**PR**	19.02727	15.55272	38.51872	0.70274	0.51311
AL4821-055	**PR**	19.02516	15.55242	38.51467	0.70274	0.51311
AL4821-058	**PR**	19.02420	15.55397	38.51810	0.70274	0.51309
AL4821-059	**PR**	19.03483	15.55759	38.52977	0.70273	0.51307
AL4820-037	**PR**	19.03263	15.55526	38.52256	0.70275	0.51311
AL4818-006	**NPR**	19.08194	15.55511	38.68403	0.70276	0.51305
AL4819-029	**NPR**	19.19415	15.57263	38.80708	0.70286	0.51298
AL4820-032	**NPR**	19.25633	15.57039	38.88095	0.70276	0.51301
AL4820-045	**NPR**	18.74816	15.52150	38.26230	0.70265	0.51310
AL4824-104	**NPR**	19.12962	15.55759	38.76151	0.70277	0.51300
AL4959-406	**NPR***	19.64512	15.59386	39.25306	0.70261	0.51302
AL4822-064	**OCC**	19.64253	15.57265	39.17994	0.70251	0.51295
AL4822-065	**OCC**	19.59033	15.57400	39.13836	0.70251	0.51299
AL4818-001	**PRTE-LV**	19.04755	15.55655	38.52138	0.70274	0.51306
AL4818-002	**PRTE-LV**	19.03735	15.55716	38.51491	0.70272	0.51306
AL4820-040	**PRTE-LV**	18.97003	15.55369	38.45631	0.70271	0.51307
AL4820-041	**PRTE-LV**	18.96176	15.54761	38.43638	0.70270	0.51307
–	–	18.95616	15.55089	38.43978	0.70271	0.51309
AL4820-043	**PRTE-LV**	18.95921	15.55021	38.45256	0.70272	0.51307
AL4821-049	**PRTE-LV**	19.01634	15.55166	38.48578	0.70272	0.51310

25,000, respectively (Fig. 4), which had previously been attributed to the existence of small-scale mantle source heterogeneities caused by variable contributions from recycled atmospheric noble gases (Péron et al., 2019). Here, we find that OCC samples exhibit a maximum $^{40}Ar/^{36}Ar$ of ~21,000, which is intermediate between the compositions of PR and PRTE-LV samples. Likewise, NPR samples show $^{40}Ar/^{36}Ar$ values that largely overlap with PRTE-LV. Taken together, these data suggest the potential existence of a $^{40}Ar/^{36}Ar$–$^{20}Ne/^{22}Ne$ continuum across mantle sources sampled at 14°N (Fig. 4a), consistent with a mantle source $^{40}Ar/^{36}Ar$ ~25,000 (Moreira et al., 1998). However, combining Ar and He isotope systematics together (Fig. 4b) reveals that $^{40}Ar/^{36}Ar$ and $^{3}He/^{4}He$ mantle source variations across PR, PRTE-LV, OCC and NPR samples are decoupled: whereas PR-affiliated and OCC samples are the most extreme mantle source end-members in He isotope space (Fig. 3), whereas OCC samples have intermediate compositions between PR and PRTE-LV samples in Ar isotope space (Fig. 4). The mantle source of OCC samples therefore appears to have a higher $^{40}Ar/^{36}Ar$ and lower $^{3}He/^{4}He$ compared to the PR mantle source.

4. Discussion

4.1. Origin of mantle source geochemical heterogeneities at 14°N

4.1.1. Occurrence of a plume-derived component

The higher $^{3}He/^{4}He$ of E-MORBs (i.e., popping rock-affiliated rocks) compared to N-MORBs (i.e., OCC) could potentially reflect a small contribution from plume-derived material, as for instance proposed in the framework of an upwelling Researcher Ridge plume material contribution (Long et al., 2019). These authors proposed that the deflection of upwelling Researcher Ridge plume material towards the west-ward migrating MAR could explain the production of E-MORBs near 14°N, with similar isotopic compositions to the Researcher Ridge lavas. However, because the $^{3}He/^{4}He$ of E-MORBs consistently remain within the canonical MORB range of 8 ± 1 R_A (Barfod et al., 1999; Graham, 2002), a plume contribution is not warranted. Graham and Michael (2021) recently hypothesized that $^{3}He/^{4}He$ variations along the East Pacific Rise (EPR) can be attributed to the partial melting of distinct mantle source compositions, involving an ultra-depleted mantle source end-member and a depleted mantle component containing percent-level contributions of enriched material. However, the He isotope systematics of E- vs. N-MORBs appears to be location-dependent. For instance, although E-MORBs from the SWIR have lower $^{3}He/^{4}He$ than associated N-MORBs (Graham et al., 2014), some E-MORBs from the southern EPR have been shown to exhibit elevated $^{3}He/^{4}He$ (Kurz et al., 2005), suggesting that the source(s) of E-MORBs may be variable. In this view, it is likely that E-MORBs do not reflect a unique noble gas end-member. It is also worth noting that there are no previous OCC noble gas measurements, so it is unclear if they are representative of OCC basalts in general, or if they are typical "normal" MORB due to the unique tectonic setting.

4.1.2. Heterogeneous recycling of surface-derived noble gases

While PR and PRTE-LV samples have trace-major element compositions and radiogenic isotope ratios pointing to a common mantle source composition (Bekaert et al, **Part A**), these samples are distinct in their bulk volatile compositions, possibly reflecting volatile element heterogeneities in their respective mantle sources. Indeed, Péron et al. (2019) previously observed the existence of a systematic difference between the mantle source $^{40}Ar/^{36}Ar$ of PR (~16,000) and PRTE-LV (~27,000) samples, which they interpreted as reflecting small-scale upper mantle heterogeneity. Due to the fact that He is not significantly entrained into the mantle during subduction (e.g., Staudacher and Allègre, 1988; Poreda & Craig, 1989; Porcelli & Wasserburg, 1995), mantle source $^{3}He/^{4}He$ variations cannot be ascribed to variable overprinting by surface-derived components. Instead, these must arise from the preservation of mantle domains with different melt and gas extraction histories, as well as variable (Th+U)/He, and radiogenic ^{4}He accumulation times. This is however not the case for Ar (and potentially Ne; Kendrick et al., 2018), implying that a mantle source with lower Ar isotopic ratios could have been more influenced by recycling of atmospheric noble gasses. Interestingly, we note that the historical PR sample 2πD43 exhibits a mantle source $^{40}Ar/^{36}Ar$ (~25,000; Moreira et al., 1998; Parai and Mukhopadhyay, 2021) that is markedly higher than other PR samples (Fig. 4), but indistinguishable from PRTE-LV samples (Péron et al., 2019). This indicates that the mantle source $^{40}Ar/^{36}Ar$ composition is not embodied in a given MORB type.

Here, our observation that He and radiogenic isotope variations do not correlate with $^{40}Ar/^{36}Ar$ (as was previously shown for some other MORBs; Sarda et al., 1999) is compatible with the $^{40}Ar/^{36}Ar$ variations near 14°N primarily arising from variable amounts of recycled atmospheric Ar in the mantle or magmatic plumbing, as previously proposed by Péron et al. (2019). One possibility is that this sea water-derived argon component originates from altered oceanic crust that would have been assimilated by the magma source of popping rocks during its

Table 2
Step crushing He and Ne analyses of PR samples analyzed in this study.

Sample	Type	weight	crushing step	$^{3}He/^{4}He$ (xRa)	1σ	^{22}Ne (x10^{-12} $cm^{3}STP/g$)	$^{20}Ne/^{22}Ne$	1σ	$^{21}Ne/^{22}Ne$	1σ
AL4818-003	**PR**	1.4	1	7.99	0.10	1.24	12.10	0.07	0.0583	0.0009
			2	8.09	0.17	2.63	12.17	0.07	0.0576	0.0008
			3	8.04	0.17	3.3	12.23	0.07	0.0570	0.0007
			4	8.06	0.12	18.2	11.94	0.06	0.0540	0.0008
			5	7.74	0.12	13.1	12.25	0.07	0.0571	0.0009
			7	8.15	0.17	2.08	12.22	0.07	0.0567	0.0009
			8	7.94	0.10	1.19	12.10	0.07	0.0563	0.0008
			9	8.04	0.08	3.57	12.17	0.07	0.0568	0.0009
			10	8.30	0.20	22.6	12.25	0.07	0.0583	0.0010
			11	8.00	0.18	8.4	11.06	0.05	0.0432	0.0004
			12	7.70	0.17	5.91	12.18	0.07	0.0579	0.0007
			13	8.15	0.18	9.63	12.26	0.07	0.0577	0.0007
			14	8.08	0.17	1.24	11.80	0.07	0.0536	0.0011
			15	8.34	0.16	11.4	12.16	0.07	0.0570	0.0008
			16	8.02	0.34	15.6	11.13	0.06	0.0461	0.0008
			17	7.93	0.15	12.0	12.20	0.07	0.0572	0.0007
			18	8.06	0.20	2.64	12.18	0.07	0.0574	0.0007
			19	8.17	0.23	2.05	12.22	0.07	0.0585	0.0009
			20	8.16	0.19	4.85	11.84	0.06	0.0531	0.0006
			21	8.24	0.18	3.96	12.17	0.07	0.0570	0.0007
			22	8.10	0.17	2.21	12.25	0.07	0.0559	0.0008
			23	8.26	0.23	8.16	12.21	0.07	0.0572	0.0006
			24	7.97	0.20	6.96	12.11	0.07	0.0568	0.0006
			25	8.02	0.22	4.93	12.06	0.07	0.0559	0.0006
			26	7.96	0.23	7.47	12.14	0.07	0.0568	0.0007
			27	7.98	0.21	5.11	12.17	0.07	0.0565	0.0007
			28	8.32	0.20	2.05	12.18	0.07	0.0582	0.0010
			29	7.99	0.19	4.42	12.24	0.07	0.0580	0.0007
AL4821-055	**PR**	1.94	1	8.01	0.20	2.42	12.29	0.07	0.0587	0.0009
			2	7.82	0.13	12.4	11.71	0.07	0.0564	0.0006
			3	7.83	0.14	6.66	11.74	0.06	0.0559	0.0007
			4	7.98	0.33	8.98	12.24	0.07	0.0597	0.0010
			5	7.93	0.17	1.47	12.19	0.07	0.0563	0.0008
			7	7.77	0.13	7.77	11.64	0.06	0.0561	0.0007
			8	8.28	0.17	1.62	11.96	0.07	0.0567	0.0009
			9	7.86	0.14	17.6	12.02	0.07	0.0576	0.0007
			10	8.05	0.16	8.98	11.93	0.07	0.0561	0.0008
			11	8.16	0.15	3.20	12.04	0.07	0.0561	0.0007
			12	8.13	0.18	3.63	12.07	0.07	0.0570	0.0008
			13	8.03	0.13	4.72	11.84	0.06	0.0545	0.0006
			14	8.03	0.16	3.3	12.10	0.07	0.0572	0.0007
			15	8.35	0.19	1.63	12.17	0.07	0.0555	0.0009
			16	7.90	0.18	2.03	12.09	0.07	0.0565	0.0009
			17	8.03	0.17	2.11	12.09	0.07	0.0565	0.0010
			18	8.08	0.16	3.88	11.93	0.07	0.0565	0.0008
			19	7.95	0.14	1.99	12.11	0.07	0.0567	0.0009
			20	7.92	0.17	2.42	12.12	0.07	0.0573	0.0009
			21	8.56	0.28	1.88	12.04	0.07	0.0571	0.0012
			22	8.34	0.27	0.83	12.10	0.07	0.0563	0.0012
			23	8.30	0.27	2.05	12.08	0.07	0.0576	0.0008
			24	8.13	0.25	5.03	11.79	0.07	0.0567	0.0006
			25	8.20	0.26	3.37	12.00	0.07	0.0575	0.0006
			26	8.12	0.28	1.73	12.11	0.07	0.0566	0.0007
			27	8.23	0.28	1.28	12.05	0.07	0.0578	0.0010
			28	8.14	0.25	0.91	12.17	0.07	0.0577	0.0008
AL4821-059	**PR**	1.40346	1	8.52	0.38	2.52	9.87	0.04	0.0292	0.0007
			2	7.79	0.20	6.34	12.19	0.07	0.0566	0.0009
			3	8.06	0.24	1.04	12.16	0.07	0.0565	0.0013
			4	8.02	0.28	1.19	10.73	0.05	0.0402	0.0011
			5	7.82	0.29	11.1	10.80	0.05	0.0400	0.0006
			7	7.29	0.25	70.4	9.92	0.04	0.0301	0.0004
			8	7.51	0.32	3.39	11.05	0.05	0.0433	0.0007
			9	7.19	0.25	1.07	12.05	0.07	0.0555	0.0013
			10	7.57	0.21	19.7	10.52	0.05	0.0361	0.0005
			11	7.28	0.19	3.91	11.72	0.06	0.0520	0.0009
			12	7.66	0.31	5.58	10.50	0.05	0.0365	0.0006
			13	8.00	0.29	11.7	10.25	0.05	0.0343	0.0005
			14	8.29	0.43	15.2	10.22	0.04	0.0328	0.0005
			15	7.48	0.23	118	9.77	0.04	0.0290	0.0004
			16	7.08	0.20	12.9	10.85	0.05	0.0407	0.0006
			17	7.28	0.24	2.82	11.90	0.06	0.0546	0.0010
			18	7.61	0.40	88.5	9.89	0.04	0.0298	0.0003
			19	8.10	0.45	0.65	12.14	0.07	0.0563	0.0014

(*continued on next page*)

Table 2 (*continued*)

Sample	Type	weight	crushing step	$^{3}He/^{4}He$ (xRa)	1σ	^{22}Ne (x10^{-12} $cm^{3}STP/g$)	$^{20}Ne/^{22}Ne$	1σ	$^{21}Ne/^{22}Ne$	1σ
			20	7.98	0.41	19.5	10.44	0.05	0.0352	0.0005
			21	8.37	0.46	45.1	10.00	0.04	0.0304	0.0003
			22	8.07	0.44	1.83	11.66	0.06	0.0515	0.0009
			23	8.21	0.48	1.58	12.06	0.07	0.0538	0.0011
			24	8.03	0.45	0.53	12.01	0.08	0.0573	0.0019
			25	8.11	0.51	1.67	10.53	0.05	0.0369	0.0009
			26	8.56	0.46	0.21	11.74	0.10	0.0523	0.0031
AL4820-037	**PR**	3.09191	1	7.92	0.10	4.91	10.87	0.05	0.0422	0.0006
			2	7.84	0.19	2.01	10.65	0.05	0.0387	0.0005
			3	7.93	0.10	12.3	10.26	0.05	0.0368	0.0005
			4	7.78	0.08	5.91	11.41	0.06	0.0521	0.0007
			5	8.22	0.17	0.79	12.13	0.07	0.0578	0.0010
			7	7.87	0.11	6.73	11.06	0.05	0.0454	0.0006
			8	7.98	0.10	6.80	10.99	0.05	0.0455	0.0006
			9	8.17	0.12	3.20	11.32	0.06	0.0538	0.0008
			10	8.22	0.12	33.4	9.78	0.04	0.0305	0.0004
			11	7.69	0.11	3.18	11.29	0.06	0.0491	0.0006
			12	7.97	0.11	2.27	11.97	0.07	0.0568	0.0008
			13	7.86	0.12	11.2	10.43	0.05	0.0373	0.0004
			14	8.10	0.13	4.22	10.23	0.05	0.0354	0.0004
			15	8.14	0.18	4.93	10.23	0.05	0.0346	0.0004
			16	7.97	0.13	1.70	12.16	0.07	0.0563	0.0007
			17	8.04	0.14	5.58	10.73	0.05	0.0406	0.0005
			18	7.95	0.15	1.68	12.16	0.07	0.0572	0.0008
			19	7.91	0.10	4.4	11.07	0.05	0.0447	0.0005
			20	8.12	0.11	1.64	12.15	0.07	0.0568	0.0007
			21	8.12	0.18	2.28	11.23	0.06	0.0465	0.0006
			22	7.93	0.11	2.01	12.08	0.07	0.0568	0.0006
			23	8.12	0.13	1.96	12.00	0.06	0.0553	0.0007
			24	8.32	0.14	3.70	10.84	0.05	0.0419	0.0005
			25	7.98	0.12	3.29	12.04	0.07	0.0567	0.0008
			26	8.29	0.17	7.01	10.25	0.05	0.0348	0.0004
			27	8.05	0.12	3.22	11.01	0.05	0.0437	0.0005
			28	8.23	0.11	1.63	12.17	0.07	0.0574	0.0008
			29	8.05	0.11	1.56	12.15	0.07	0.0570	0.0009
			30	8.19	0.16	4.79	10.47	0.05	0.0365	0.0004
			31	8.36	0.21	1.15	12.02	0.07	0.0563	0.0009
			32	8.01	0.12	3.15	11.17	0.06	0.0464	0.0005
			33	8.19	0.12	2.58	11.37	0.06	0.0487	0.0007
			34	8.03	0.11	1.93	11.98	0.06	0.0557	0.0008

ascent through the crust, which is potentially consistent with the slightly lower maximum $^{20}Ne/^{22}Ne$ of PR analyzed in this study compared to other samples (Fig. 4a). Another possibility is that the continuum of mantle source $^{40}Ar/^{36}Ar$–$^{20}Ne/^{22}Ne$ observed near 14°N (Fig. 4) primarily reflects variable degrees of atmospheric contamination during lava emplacement at the seafloor. Péron et al. (2019) however ruled out this later scenario by pointing out a remarkable agreement between bulk measurements and laser ablation data, and arguing that contamination by atmospheric gas should not be pervasive enough to uniformly affect the samples. If correct, this indeed suggests that subduction of atmosphere-derived Ar (and potentially Ne) and/or assimilation of sea water-bearing altered oceanic crust are the two most likely processes for generating apparent mantle source heterogeneities along a mid-ocean ridge, by variably reducing mantle $^{40}Ar/^{36}Ar$ (and $^{20}Ne/^{22}Ne$) (e.g., Sarda et al., 1999; Parai et al., 2012; Tucker et al., 2022; Holland and Ballentine, 2006). We note however that noble gas analyses of individual popping rock vesicles by Burnard et al. (1997) showed a large variability of $^{40}Ar/^{36}Ar$, from ~4000 to ~40,000, suggesting that a large fraction of ^{36}Ar released from popping rocks may actually originate from surface-adsorbed atmospheric Ar, and implying that the mantle source $^{40}Ar/^{36}Ar$ is likely higher (≥40,000, Burnard *et al.* (1997); but arguably ≤ 44,000, Moreira et al., 1998) than derived from step crushing experiments (≤25,000; Fig. 4a).

4.1.3. Occurrence of a recycled, sedimentary component

By analogy with He isotopes, N isotopes have the potential to distinguish between convecting mantle and plume-derived mantle source contributions. Historically, an isotopically heavy $\delta^{15}N$ has been defined for the deep mantle (typically ~ +3‰; Marty and Dauphas, 2003) and attributed to the introduction of subducted sediments (Cartigny and Marty, 2013; Barry and Hilton, 2016; Bekaert et al., 2021b), which are enriched in ^{15}N relative to the atmospheric composition ($\delta^{15}N$ = +3 to +7 ‰; Peters et al., 1978; Kienast, 2000). Likewise, it has been proposed that the $\delta^{15}N$ of E-MORBs could be as high as +2 ‰ (e.g., Cartigny et al., 2001), i.e., much higher than the canonical upper mantle (-5 ± 2 ‰), due to the pervasive addition of recycled N with positive $\delta^{15}N$. However, Labidi (2022) recently provided an in-depth comparison of $\delta^{15}N$ and $N_2/^{3}He$ systematics in low ($^{3}He/^{4}He < 8*R_A$) and high ($^{3}He/^{4}He > 8*R_A$) $^{3}He/^{4}He$ mantle plume sources, demonstrating that positive $\delta^{15}N$ signatures are likely restricted to low $^{3}He/^{4}He$ sources akin to that sampled by the Society plume (i.e., with conspicuous geochemical evidence for recycled material contribution, including detrital sediments; e.g., Chauvel et al., 1992). The average $\delta^{15}N$ signature of high $^{3}He/^{4}He$ sources may thus be intermediate between low $^{3}He/^{4}He$ plume sources and the ^{15}N-depleted convecting mantle (Labidi, 2022). The potential occurrence of $^{3}He/^{4}He$ mantle plume sources with positive $\delta^{15}N$ compositions has been suggested based on the analysis of Icelandic volcanic glasses (with $\delta^{15}N$ up to +5.71 ‰; Halldórsson et al., 2016), but the low $^{40}Ar/^{36}Ar$ of these samples suggests these signatures may not represent a deep signature.

In any case, the observation of a homogeneous $\delta^{15}N$ (=−4.49 ± 1.40 ‰; Table 4) across the full range of MORB compositions (i.e., form N-MORBs to E-MORBs) implies that N isotopes are not sensitive to mantle source heterogeneities at 14°N, and that there is no clear evidence for the occurrence of recycled sedimentary N or plume-derived N in the mantle source of MORBs near 14°N on the MAR. This conclusion appears

Table 3
Step crushing He and Ne analyses of NPR samples analyzed in this study.

Sample	Type	weight	crushing step	$^{3}He/^{4}He$ (xRa)	1σ	^{22}Ne (x10^{-12} $cm^{3}STP/g$)	$^{20}Ne/^{22}Ne$	1σ	$^{21}Ne/^{22}Ne$	1σ
AL4818-006	**NPR**	2.21	1	7.95	0.20	0.69	10.59	0.05	0.0373	0.0007
			2	7.57	0.34	0.23	11.12	0.08	0.0475	0.0016
			3	7.87	0.21	0.68	10.79	0.05	0.0403	0.0009
			4	7.88	0.22	0.65	10.48	0.05	0.0369	0.0011
			5	7.82	0.2	1.03	10.55	0.05	0.0376	0.0009
			6	7.97	0.19	0.65	10.33	0.05	0.0336	0.0009
AL4819-029	**NPR**	3.21032	1	7.66	0.15	0.73	11.24	0.06	0.0452	0.0009
			2	7.64	0.15	0.78	12.26	0.07	0.0558	0.0012
			3	7.82	0.14	0.94	11.86	0.06	0.0513	0.0008
			4	7.65	0.12	1.11	12.04	0.06	0.0542	0.0009
			5	7.53	0.13	0.82	12.02	0.06	0.0533	0.0011
			6	7.51	0.08	1.46	11.87	0.06	0.0529	0.0009
			7	7.67	0.08	1.74	11.2	0.06	0.0446	0.0006
			8	7.67	0.11	1.46	11.32	0.06	0.0461	0.0008
			9	7.50	0.11	0.58	10.97	0.06	0.0421	0.0011
AL4820-045	**NPR**	2.45725	1	7.85	0.14	3.65	9.86	0.04	0.0300	0.0004
			2	8.13	0.15	1.08	10.18	0.04	0.0331	0.0005
			3	8.20	0.2	0.47	11.38	0.06	0.0479	0.0011
			4	8.00	0.21	0.43	11.13	0.06	0.042	0.0008
			5	8.04	0.15	1.88	11.45	0.06	0.0466	0.0005
			6	8.25	0.17	4.18	10.07	0.04	0.0323	0.0004
			7	8.13	0.14	0.14	12.23	0.08	0.0535	0.0015
			8	8.26	0.21	1.68	10.49	0.05	0.0353	0.0004
AL4824-104	**NPR**	1.1409	1	7.62	0.12	0.67	11.03	0.07	0.0431	0.0019
			2	7.56	0.18	1.33	11.37	0.06	0.0478	0.0013
			3	7.60	0.22	2.58	10.69	0.05	0.0394	0.0012
			4	7.56	0.16	1.94	10.99	0.06	0.042	0.0009
			5	7.45	0.25	1.54	11.24	0.06	0.0447	0.0013
			6	7.59	0.24	9.45	10.32	0.05	0.0336	0.0005
			7	7.51	0.14	1.67	10.6	0.05	0.0366	0.0009
			8	7.81	0.16	1.56	10.38	0.05	0.0349	0.0012
AL4959-406	**NPR***	2.14152	1	7.20	0.18	0.61	12.42	0.07	0.0569	0.0012
			2	7.03	0.19	7.12	9.92	0.04	0.0305	0.0004
			3	7.11	0.16	0.95	12.21	0.07	0.0544	0.0010
			4	7.20	0.19	0.67	11.7	0.06	0.0485	0.0013
			5	7.22	0.19	1.35	12.25	0.07	0.0551	0.0008
			6	7.20	0.24	0.32	12.2	0.08	0.0527	0.0010
			7	7.31	0.27	1.45	11.82	0.06	0.0503	0.0007
			8	7.21	0.18	0.94	11.82	0.06	0.05	0.0006
			9	7.09	0.2	0.46	11.7	0.07	0.0458	0.0010

Table 4
Step crushing He and Ne analyses of OCC samples analyzed in this study.

Sample	Classification	weight	crushing step	$^{3}He/^{4}He$ (xRa)	1σ	^{22}Ne (x10^{-12} $cm^{3}STP/g$)	$^{20}Ne/^{22}Ne$	1σ	$^{21}Ne/^{22}Ne$	1σ
AL4822-064	**OCC**	1.19782	1	7.00	0.16	1.48	12.48	0.07	0.0569	0.0013
			2	6.63	0.17	1.20	12.43	0.07	0.0573	0.0012
			3	6.77	0.11	0.47	12.25	0.08	0.0467	0.0045
			4	6.77	0.13	0.57	12.12	0.08	0.0559	0.0017
			5	6.79	0.19	22.6	9.90	0.04	0.0295	0.0004
AL4822-065	**OCC**	0.9391	1	6.74	0.13	37.1	9.86	0.04	0.0298	0.0004
			2	6.97	0.14	0.70	12.28	0.08	0.0563	0.0014
			3	6.82	0.18	1.76	12.34	0.07	0.0565	0.0015
			4	6.91	0.12	0.62	12.35	0.09	0.0550	0.0029
			5	6.80	0.14	0.53	12.29	0.09	0.0533	0.0020
			6	6.56	0.13	0.03	11.54	0.93	0.0557	0.0145

also consistent with $\Delta^{207}Pb/^{204}Pb$– $\Delta^{208}Pb/^{204}Pb$ systematics, which tracks the distribution of recycled sediments across the mantle (Hart, 1984; Jackson et al., 2007) (Fig. 5). The Δ Pb isotope systematics of MORB samples from 14°N on the MAR displays no evidence for a contribution of marine sedimentary material in the corresponding mantle sources (Fig. 5). At first order, MORB samples at 14°N on the MAR define a broad trend from DMM values towards a low $\Delta^{207}Pb/^{204}Pb$ end-member (that still remains in the range of previously analyzed MORBs). Because only "young HIMU" samples (HIMU = "high-μ", whereby $\mu = {}^{238}U/^{204}Pb$; Zindler and Hart, 1986) are known to consistently harbor negative $\Delta^{207}Pb/^{204}Pb$ values (e.g., Thirlwall, 1997), there is a potential for OCC samples with low $\Delta^{207}Pb/^{204}Pb$ values to reflect a slight addition of a young HIMU-type flavor. The exact nature of the additional mantle component found in OCC samples however remains uncertain.

4.1.4. Occurrence of a recycled, crustal ("young" HIMU-type) component in OCC samples?

OCC samples (classified as N-MORBs according to their trace and major element ratios; Bekaert et al., **Part A**) have more radiogenic Pb and Nd isotope compositions than PR-affiliated samples (which are classified as E-MORBs). Typically, N-MORBs are characterized by (La/

Table 5
Step crushing He and Ne analyses of PRTE-LV samples analyzed in this study.

Sample	Classification	weight	crushing step	$^{3}He/^{4}He$ (xRa)	1σ	^{22}Ne (x10^{-12} $cm^{3}STP/g$)	$^{20}Ne/^{22}Ne$	1σ	$^{21}Ne/^{22}Ne$	1σ
AL4818-002	**PRTE-LV**	1.37599	1	7.90	0.17	0.98	11.26	0.06	0.0452	0.0008
			2	8.00	0.17	1.24	12.32	0.07	0.0569	0.0007
			3	8.23	0.21	1.04	12.28	0.07	0.0572	0.0010
			4	8.04	0.19	0.73	12.14	0.07	0.0563	0.0011
AL4820-043	**PRTE-LV**	0.96187	1	8.31	0.13	1.63	11.53	0.07	0.0490	0.0009
			2	8.33	0.26	17.8	10.09	0.04	0.0319	0.0003
			3	7.83	0.25	29.3	9.87	0.04	0.0295	0.0003
			4	7.69	0.25	16.2	9.73	0.04	0.0291	0.0003
			5	8.27	0.20	5.70	12.66	0.07	0.0596	0.0007
			7	8.27	0.14	6.38	12.56	0.07	0.0594	0.0006
			8	8.13	0.20	4.81	12.45	0.07	0.0587	0.0007
			9	8.40	0.20	6.60	12.54	0.07	0.0591	0.0007
			10	8.18	0.22	45.0	9.55	0.04	0.0316	0.0004
			11	8.05	0.19	13.6	11.12	0.05	0.0411	0.0005
			12	8.10	0.24	3.66	12.54	0.07	0.0585	0.0008
			13	8.09	0.24	8.06	11.38	0.06	0.0462	0.0006
			14	8.23	0.21	4.04	12.20	0.07	0.0554	0.0006
			15	8.03	0.25	2.80	12.48	0.07	0.0588	0.0010
			16	8.04	0.24	2.28	12.52	0.07	0.0586	0.0009
			17	8.44	0.23	11.7	10.75	0.05	0.0392	0.0005
			18	8.15	0.23	2.54	12.48	0.07	0.0589	0.0010
			19	8.06	0.25	1.74	12.52	0.07	0.0602	0.0011

Table 6
Summary of helium isotope and concentration data for MORB samples analyzed in this study, by combined (single step) crushing and melting of the remaining powder.

Sample	Classification	$^{3}He/^{4}He$ (R/R_A)	Error (1σ)	Bulk ^{4}He (ccSTP/g)	^{4}He fraction released upon crushing
AL4818-003	**PR**	8.22	0.11	6.77x10^{-05}	99 %
AL4821-055	**PR**	8.25	0.11	3.38x10^{-05}	97 %
AL4821-058	**PR**	8.02	0.10	4.47x10^{-05}	98 %
AL4821-059	**PR**	7.67	0.10	6.77x10^{-05}	99 %
AL4820-037	**PR**	8.07	0.10	2.67x10^{-05}	97 %
AL4818-006	**NPR**	7.66	0.10	3.56x10^{-06}	63 %
AL4819-029	**NPR**	7.77	0.11	1.22x10^{-05}	85 %
AL4820-032	**NPR**	7.43	0.09	1.35x10^{-06}	3 %
AL4820-045	**NPR**	7.69	0.11	1.22x10^{-05}	48 %
AL4824-104	**NPR**	7.65	0.10	8.68x10^{-06}	92 %
AL4959-406*	**NPR**	7.18	0.08	2.15x10^{-06}	–
AL4822-064	**OCC**	6.64	0.09	5.64x10^{-06}	83 %
AL4822-065	**OCC**	6.84	0.08	1.11x10^{-05}	83 %
AL4818-001	**PRTE-LV**	8.16	0.11	8.03x10^{-06}	69 %
AL4818-002	**PRTE-LV**	7.77	0.10	4.77x10^{-06}	55 %
AL4820-040	**PRTE-LV**	8.25	0.10	3.48x10^{-05}	95 %
AL4820-041	**PRTE-LV**	8.10	0.12	3.63x10^{-05}	96 %
replicate	**–**	–	–	–	–
AL4820-043	**PRTE-LV**	8.04	0.12	4.58x10^{-05}	97 %
AL4821-049	**PRTE-LV**	8.45	0.10	4.97x10^{-06}	41 %

$Sm)_{ch.} < 1$, $K_2O/TiO_2 < 0.11$ (Fig. 6) and isotopic compositions reflecting long-term depletion in the more incompatible elements (i.e., high $^{143}Nd/^{144}Nd$, low$^{87}Sr/^{86}Sr$, low$^{206}Pb/^{204}Pb$). Conversely, E-MORBs are enriched in the incompatible elements (e.g., $(La/Sm)_{ch.} > 1.7$, $K_2O/TiO_2 > 0.2$; Fig. 6) as a result of a low degree partial melting and/or geochemical enrichment of the mantle source. Their isotope ratios also suggest less long-term depletion of the most incompatible element (e.g., low$^{143}Nd/^{144}Nd$, high$^{87}Sr/^{86}Sr$, high$^{206}Pb/^{204}Pb$) compared to N-MORBS (Fig. 2). If the mantle sources of PR-affiliated and OCC samples were to be compositionally identical, then the low $(La/Sm)_{ch.}$ and K_2O/TiO_2 of OCC samples ($(La/Sm)_{ch.} < 0.7$) could indicate a higher degree of partial melting compared to PR-affiliated samples ($(La/Sm)_{ch.} > 1.8$; Fig. 6**)**. However, conspicuous evidence for the existence of geochemical heterogeneities near 14°N on the MAR (e.g., as seen through the Pb, Sr, and Nd isotope variations; Figs. 2–3) suggest that $(La/Sm)_{ch.}$ and K_2O/TiO_2 variations may primarily reflect local mantle source geochemical variations rather than variable degrees of partial melting. Further support for mantle heterogeneities near 14°N on the MAR is found in the high Dy/Yb of OCC samples relative to other MORB samples **(**Fig. 6**),** suggesting the presence of garnet (which retains the heavy REE in preference to middle and light REE during mantle melting at depth (garnet stability field)) in the source of the OCC samples.

Taken together with the lower $^{3}He/^{4}He$ of the mantle source of OCC samples compared to other MORBs at 14°N on the MAR, the geochemical characteristics of OCC samples (e.g., low Δ $^{207}Pb/^{204}P$, $^{143}Nd/^{144}Nd$ and $^{87}Sr/^{86}Sr$) are potentially consistent with a slight addition of a ("young") HIMU-type "flavor", widely thought to originate from oceanic crust recycling (Chauvel et al., 1992). HIMU-type MORBs are indeed considered to have lower radiogenic noble gas isotopic ratios than typical MORBs, with mantle source $^{3}He/^{4}He \sim 4.5$ Ra and $^{40}Ar/^{36}Ar$ about 18,100 ± 600 (Hanyu and Kaneoka, 1997; Barfod et al., 1999; Moreira and Kurz, 2001; Day and Hilton, 2011; Hanyu et al., 2011; Tucker et al., 2012). Interestingly, the nitrogen isotope composition of the "recycled oceanic crust" component is poorly constrained and highly variable (e.g., Li et al., 2007; Busigny et al., 2019), although the analysis of alpine ophiolites also suggests slightly positive $\delta^{15}N$ around 2.8 ± 1.2 ‰ (1σ) (Busigny et al., 2011). A contribution from a ^{15}N-rich component in OCC samples is thus not evident from our N isotope measurements (Table 4).

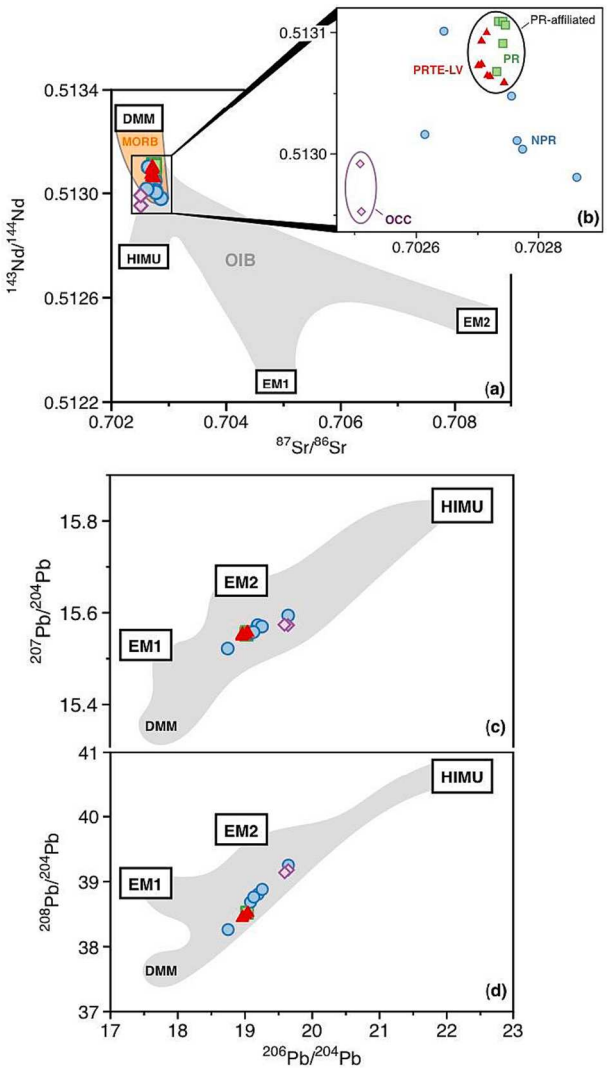

Fig. 2. Radiogenic isotope variations in MORB samples analyzed in this study. End-member compositions from Hofmann (2007) do not include extreme EM2 samples reported by Jackson et al. (2007). The grey areas represent the contours of the available data (Hofmann, 2007) that were assembled from the GEOROC database. Panel (b) shows a zoomed-in view of the data presented in this study in Nd versus Sr isotope space, emphasizing the distinct composition of OCCs relative to PR-affiliated samples.

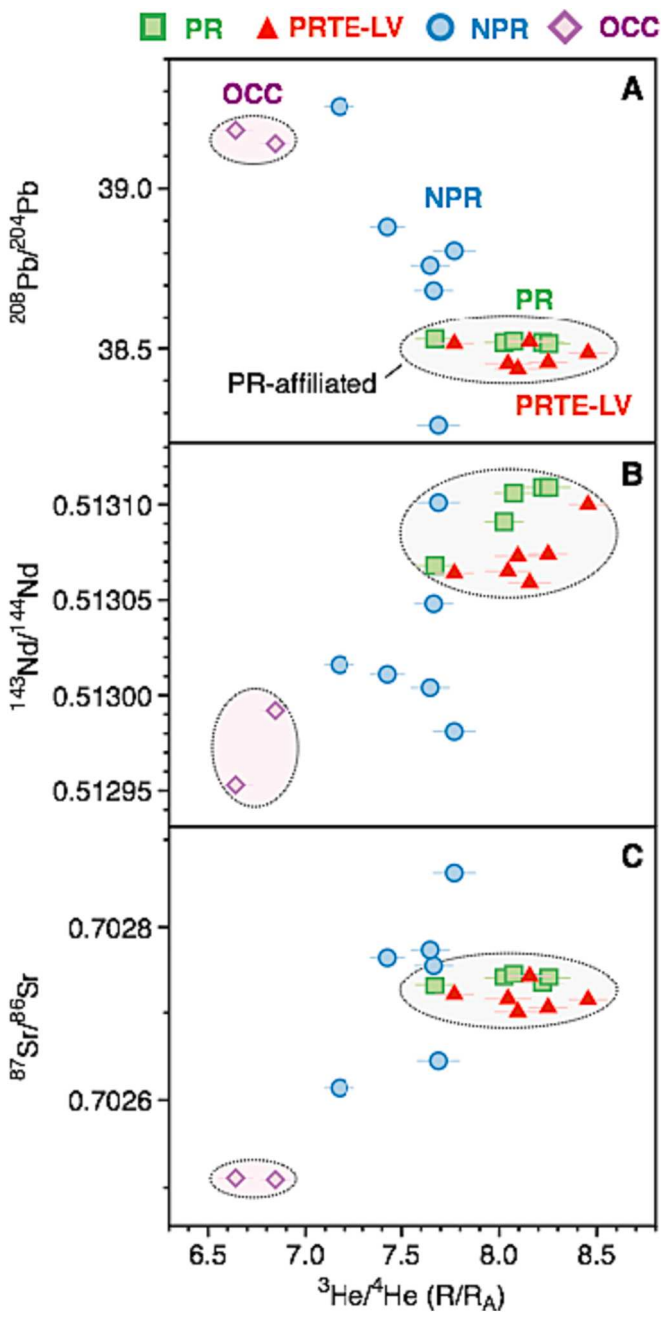

Fig. 3. Co-variations of radiogenic (Table 1) and He (Tables 2–6) isotope data in MORB samples near 14°N on the MAR. Co-variations between He isotope and radiogenic isotope data across the (n = 19) MORB samples analyzed in this study suggest that He isotope variations near 14°N reflect mantle source heterogeneities. The two dashed circles represent the two compositional end-members corresponding to OCC and popping rock-affiliated (PR-affiliated) samples. NPR samples have intermediate compositions between these two endmembers.

4.2. Origin of C and N within the convecting mantle

4.2.1. Mantle source $C/^3He$, C/N, and $N_2/^3He$ variations

MORB samples analyzed in this study exhibit highly variable C/N (in the range 125–4580), spanning the entire range from N-MORB-like (i.e., 273 ± 106) to E-MORB-like (i.e., 1839 ± 641) values (Marty et al., 2020) (Fig. 7, Fig. 9, **Bekaert et al., Part A**). Importantly, and regardless of the assumed $^4He/^{40}Ar^*$ production ratio (**scenario A or B; Bekaert et al., Part A**), we confirm previous findings by (Marty, 2012) (Marty et al., 2020) that the C/N of the MORB mantle is markedly higher (≥90) than that of the surface reservoir (C/N = 21 ± 6; Bergin et al., 2015; Hirschmann, 2018). This finding is important, as the C/N of the bulk silicate Earth remains a subject of ongoing debate, with estimates ranging from 61 ± 23 (where mantle carbon concentrations are obtained from calibration to Ba (Bergin et al., 2015)) up to 365 ± 233 (from the analysis of CO_2 and N_2 in MORBs and oceanic island basalts; Marty and Zimmermann, 1999; Marty and Dauphas, 2003; Marty, 2012). The heterogeneous nature and higher C/N of the MORB mantle relative to that of the surface inventory has notably been proposed to reflect the preferential subduction of C compared to N (Marty and Zimmermann, 1999). Considering the analysis of CO_2-rich gases worldwide for which a mantle origin has been determined using noble gas isotopes, Marty et al. (2020) confirmed that the mantle consistently exhibits high C/N relative to the surface inventory, pointing towards a unique volatile composition when compared to potential cosmochemical accretionary endmembers. These authors thus proposed an alternative possibility for explaining the high C/N of the BSE, suggesting it could have been inherited from evolved planetary precursors depleted in

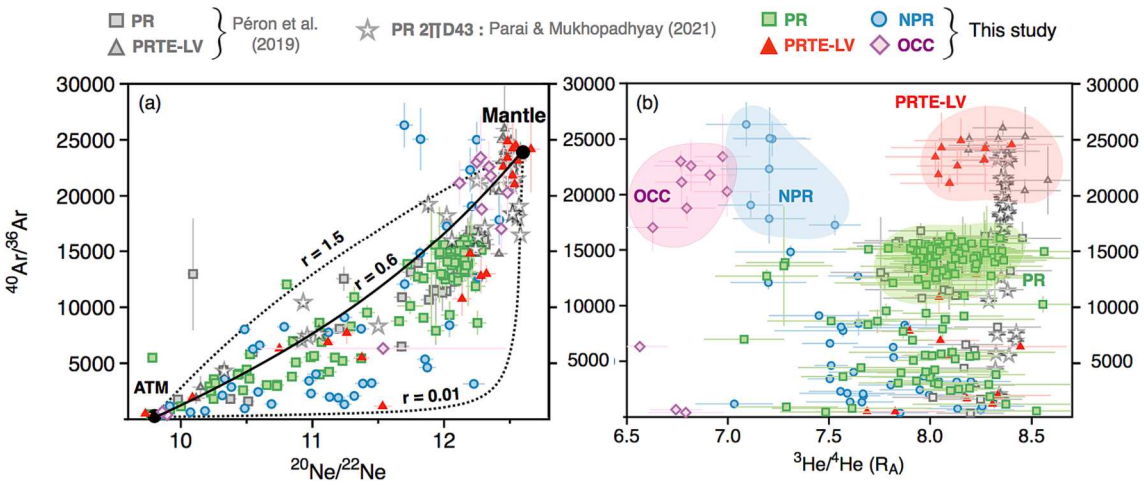

Fig. 4. He-Ne-Ar isotope variations during stepwise crushing of MORB samples analyzed in this study. (a) The $^{40}Ar/^{36}Ar$ composition of the mantle source (i.e., at $^{20}Ne/^{22}Ne$~12.6) of OCC samples appears intermediate between the mantle source compositions of PR (~16,000) and PRTE-LV (~27,000) (Péron et al., 2019). Broad regions indicative of mantle source compositions for OCC (purple), NPR (blue), PR (green) and PRTE-LV (red) samples are reported as colored areas on panel b. As suggested by Parai and Mukhopadhyay (2021), a significant fraction of the scatter in the data likely reflects contribution from multiple atmospheric contaminants with varying $^{36}Ar/^{22}Ne$ ratios. Bounds on mixing hyperbolae between atmosphere (ATM) and mantle source (Mantle) components from Parai and Mukhopadhyay (2021) are shown for reference ($r = (^{36}Ar/^{22}Ne)_{mantle}/(^{36}Ar/^{22}Ne)_{air}$, also referred to as the curvature parameter). (b) Whereas PR and PRTE-LV samples define two distinct mantle source $^{40}Ar/^{36}Ar$, they share a common mantle source $^{3}He/^{4}He$ at ~ 8.2 R_A. $^{40}Ar/^{36}Ar$ and $^{3}He/^{4}He$ mantle source variations for PR, PRTE-LV, OCC and NPR samples appear to be decoupled, suggesting that mantle source $^{40}Ar/^{36}Ar$ variations have a distinct origin from mantle source $^{3}He/^{4}He$ variations. The historical PR sample 2πD43 exhibits a mantle source $^{40}Ar/^{36}Ar$ that is markedly higher than other PR samples (i.e., ~25,000 (Moreira et al., 1998), here shown using data from Parai and Mukhopadhyay (2021)) but indistinguishable from PRTE-LV samples (Péron et al., 2019), indicating that the mantle source $^{40}Ar/^{36}Ar$ composition is not representative of a given MORB type. (For interpretation of the references to colour in this figure legend, the reader is referred to the web version of this article.)

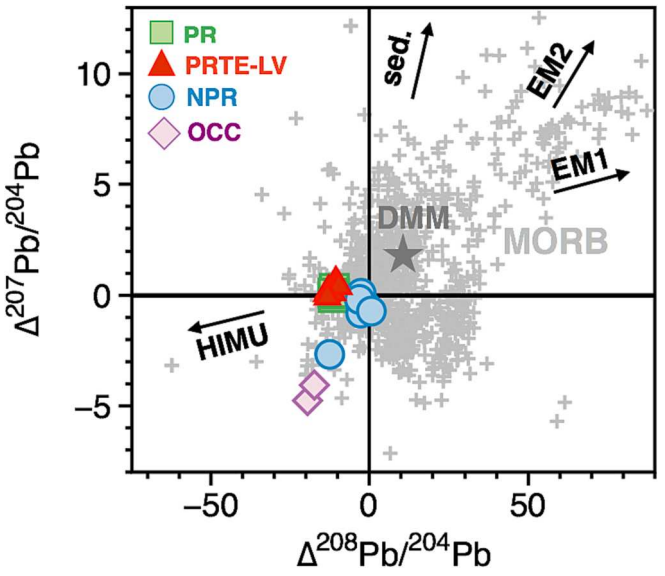

Fig. 5. ΔPb isotope compositions of MORB samples analyzed in this study, indicating the clear absence of a significant contribution from recycled marine sediments in the corresponding mantle source(s). ΔPb corresponds to the delta deviation from the Northern Hemisphere Regression Line of Hart (1984). Figure adapted from Jackson et al. (2007), using MORB data from Stracke (2012) for comparison. Pb isotope data for mantle endmembers DMM, EM1 (Pitcairn), EM2 (Society,Samoa), and HIMU (Mangaia and Tubuai) are reproduced from Jackson et al. (2007).

volatile and moderately volatile elements, rather than the result of terrestrial differentiation and evolution. A third possibility is that the high C/N ratios across the solid Earth could also - at least partially - result from the preferential sequestration of N in planetary cores compared to C during planetesimal differentiation and/or Earth's core formation (Marty, 2012; Roskosz et al., 2013). More experimental work is however needed to investigate the role of pressure and bulk chemical composition on the metal-silicate partitioning of N compared to C (Dalou et al., 2017; Grewal et al., 2020). In this framework, and given the multiplicity of processes that could have contributed to increasing the C/N of mantle reservoirs, the relative efficiencies of C and N recycling remain open to debate (Bekaert et al., 2021b).

After correction for solubility-controlled fractionation (assuming a $^{4}He/^{40}Ar^{*}$ production ratio = 1; Bekaert *et al.*, **Part A**), we find that $C/^{3}He_{4/40}$ and $C/N_{4/40}$ ratios at 14°N on the MAR generally do not correlate with the degree of geochemical enrichment, with the potential exception of NPR samples (coefficients of determination for $C/^{3}He_{4/40}$ and $C/N_{4/40}$ versus K_2O/TiO_2 are 0.50 and 0.94, respectively; Fig. 7). Correcting the $C/^{3}He$ values for solubility-controlled fractionation assuming a $^{4}He/^{40}Ar^{*}$ mantle production ratio of 3 would only marginally affect this result (Fig. 9 in Bekaert *et al.*, **Part A**), yielding average $C/^{3}He_{4/40}$ of $(2.81 \pm 0.46) \times 10^{9}$, $(2.18 \pm 0.19) \times 10^{9}$, $(2.09 \pm 0.29) \times 10^{9}$, and $(2.99 \pm 0.41) \times 10^{9}$ for PR, PRTE-LV, OCC and NPR samples, respectively. These data therefore suggest limited (if any) difference between the $C/^{3}He$ ratios of N-MORB and E-MORB mantle sources near 14°N, with an average pre-degassing MORB $C/^{3}He$ of $(2.65 \pm 0.51) \times 10^{9}$. This estimate is indistinguishable from the previously proposed average $C/^{3}He_{4/40}$ of all MORB types ($(2.2 \pm 0.6) \times 10^{9}$; Marty and Zimmermann, 1999), and slightly higher than the average pre-degassing MORB $C/^{3}He$ ratio of $(1.67 \pm 0.21) \times 10^{9}$ proposed by Tucker et al. (2018). Considering a pre-degassing MORB $C/^{3}He$ of $(2.65 \pm 0.51) \times 10^{9}$, a ^{3}He flux of 800 mol/year, a degree of mantle partial melting of 12 %, and a magma generation rate at ridges of 20 km^3/yr (e.g., Marty, 2012; Bekaert et al., 2021b) yields an upper mantle C flux from ridges of $(2.12 \pm 0.41) \times 10^{12}$ mol/yr. This value is consistent with previous estimates of $1.32^{+0.77}_{-0.85} \times 10^{12}$ mol/yr and $2.3^{+2.7}_{-1.3} \times 10^{12}$ from Le Voyer et al. (2019) and Cartigny et al. (2008) and a homogeneous MORB mantle C concentration of 50 ± 10 ppm, indistinguishable from previous estimate of Marty (2012). The absence of significant difference

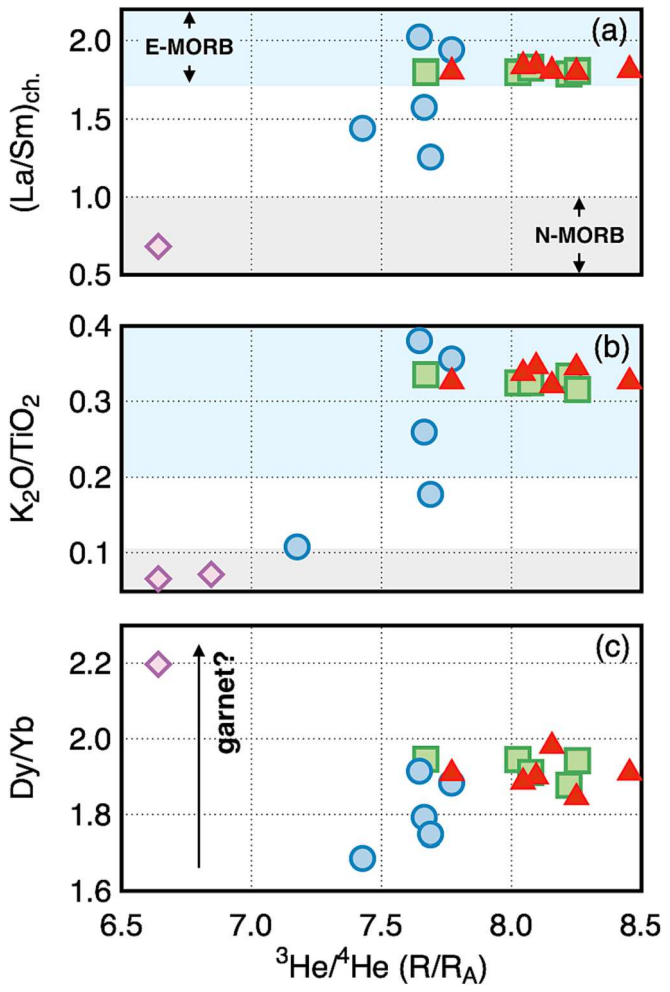

Fig. 6. He isotope ratios as a function of $(La/Sm)_{ch.}$ (a), K_2O/TiO_2 (b), and Dy/Yb (c) in MORB samples analyzed in this study.

in the C concentration of N-MORBs and E-MORBs near 14°N appears at odds with the proposal of a systematic difference between these two end-members (i.e., 30 ± 10 ppm C and 140 ± 30 ppm C for N-MORB and E-MORB, respectively (Marty, 2012)). This suggests that "E-MORB" may not be a unique mantle end-member, and that the multiplicity of mantle sources and processes contributing to MORB generation at 14° N on the MAR may produce a geochemical enrichment that is specific to this location.

The absence of a clear correlation between $C/N_{4/40}$ – $C/^3He_{4/40}$ ratios and the degree of MORB enrichment (Fig. 7) suggests that the geochemical enrichment carried out by PR-related samples near 14°N on the MAR is not associated with recycling of a C-rich component with a high C/N, as was suggested for other MORB samples worldwide (Marty and Zimmermann, 1999). The good correlation between $C/N_{4/40}$ and K_2O/TiO_2 (R^2 = 0.94, Fig. 7c) for NPR samples however appears compatible with the proposal of a geochemical enrichment associated with recycling of a C-rich component (Marty and Zimmermann, 1999), implying that the geochemical enrichment observed for some NPR samples may have a distinct origin from that of PR-related samples. This could notably indicate that several processes and/or sources are contributing to the geochemical enrichments at 14°N on the MAR.

These results do not preclude the possibility that at least a portion of the C within the upper mantle originates from recycling. As recently pointed out by Graham and Michael (2021), the common $C/^3He$ ratio of 2×10^9 generally ascribed to the upper mantle source for MORBs may actually reflect the pervasive and homogeneous overprinting of mantle carbon by a recycled, carbon-rich component. Assuming that the baseline $C/^3He$ ratio of the upper mantle is on the order of 3×10^8 or less (Graham and Michael, 2021), this could imply that most of the C in Earth's upper mantle actually originates from recycling. Also note that extrapolation of regional observations (e.g., near 14°N on the MAR) to the global upper mantle is highly uncertain as local mantle source heterogeneities exist and can be seen through the lens of other geochemical proxies (section 4.1.5.). Thus, the absence of carbon enrichment in the mantle source near 14°N does not exclude the possibility for high $C/^3He$ in other regions to represent more prominent inputs of recycled C.

Combining $C/^3He$ with C/N systematics, we derive estimates for the $N_2/^3He$ of the samples analyzed in this study. We observe an inverse correlation between $N_2/^3He$ and $^4He/^{40}Ar^*$, in line with expectations for fractional degassing. Correcting the $N_2/^3He$ using a mantle $^4He/^{40}Ar^*$ production ratio of 3 or 1 (**scenarios A and B** from Bekaert et al., **Part A**,

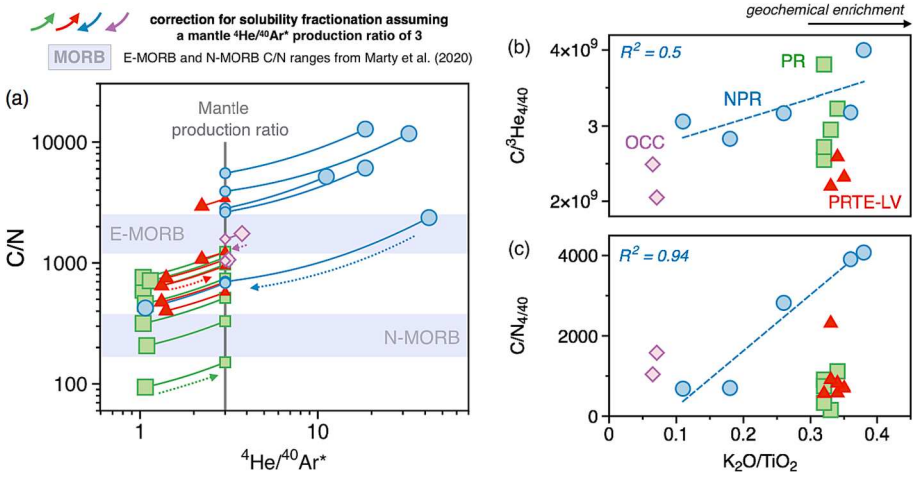

Fig. 7. C/N-$^4He/^{40}Ar^*$ systematics of MORB samples analyzed in this study. $C/N_{4/40}$ values, computed by assuming a $^4He/^{40}Ar^*$ mantle production ratio of 3 (Fig. 9; Bekaert et al., Part A), are represented as small symbols. We find that the $C/N_{4/40}$ values of NPR are generally higher than NPR, with $C/N_{4/40}$ values of PRTE-LV and OCC samples being intermediate between these two end-members. E-MORB and N-MORB C/N ranges from Marty et al. (2020) are shown for comparison. We observe no clear correlation between the $C/^3He_{4/40}$ (b) and $C/N_{4/40}$ (c) of MORB samples analyzed in this study and their degrees of geochemical enrichment represented by the K_2O/TiO_2, with the potential exception of NPR samples (dashed lines with coefficients of determination of 0.50 and 0.94 for $C/^3He_{4/40}$ (b) and $C/N_{4/40}$ (c) versus K_2O/TiO_2, respectively).

respectively) reduces the discrepancies observed across $N_2/^3He$ of MORB samples analyzed in this study, suggesting that a significant fraction of the observed variability arises from solubility controlled fractionation. In line with $C/^3He_{4/40}$ and $C/N_{4/40}$ systematics (Fig. 7), we find that $N_2/^3He_{4/40}$ variations at 14°N on the MAR generally do not correlate with the degree of geochemical enrichment, with again the potential exception of NPR samples (coefficients of determination for $N_2/^3He_{4/40}$ versus K_2O/TiO_2 of 0.88; Fig. 8b,c). In agreement with Marty and Zimmermann (1999), we find that the correlation between $N_2/^3He_{4/40}$ and K_2O/TiO_2 for NPR samples may even be slightly negative. One PR sample (AL4818-003) exhibits a $N_2/^3He_{4/40}$ that is markedly higher than any other sample analyzed in this study. Excluding this sample yields an average $N_2/^3He$ of $(5.5 \pm 3.8)x10^6$ and $(1.1 \pm 0.8)x10^7$, for mantle $^4He/^{40}Ar^*$ production ratios of 3 and 1, respectively. These estimates are slightly higher than (but within error of) previous estimates for the $N_2/^3He$ of the convecting mantle from all types of MORBs worldwide ($(4.37 \pm 1.64)x10^6$, Marty and Zimmermann, 1999; $(3.7 \pm 1.2)x10^6$, Labidi (2022)). This apparent homogeneity of both $N_2/^3He$ and $\delta^{15}N$ across mantle source reservoirs with variable degrees of geochemical enrichment has been considered as precluding significant contribution of subduction-derived N to the overall budget of N within the Earth's mantle (Labidi, 2022). If correct, this would imply that the homogeneous $N_2/^3He$ and $\delta^{15}N$ of the convecting mantle represent primordial signatures, predating the onset of subduction (Labidi, 2022).

4.2.2. How to explain the N isotope homogeneity of the upper mantle?

The average $\delta^{15}N$ value of -4.49 ± 1.40 ‰ at 14°N (Fig. 9) appears consistent with previously published nitrogen isotope data for popping rocks (Javoy and Pineau, 1991; Labidi et al., 2020) and other upper mantle-derived samples (e.g., diamonds; Cartigny and Marty (2013)), but inconsistent with the proposal of a positive (~ +2 ‰) $\delta^{15}N$ value for the E-MORB end-member (Marty and Humbert, 1997; Marty and Zimmermann, 1999; Sano et al., 1998; Nishio et al., 1999; Cartigny et al., 2001). The striking $\delta^{15}N$ homogeneity of MORB samples with highly variable K_2O/TiO_2 indicates the processes and/or sources contributing to the geochemical enrichments at 14°N on the MAR did not modify their N isotope compositions. High K_2O/TiO_2 lavas worldwide appear to be associated with a diverse range of incompatible element signatures

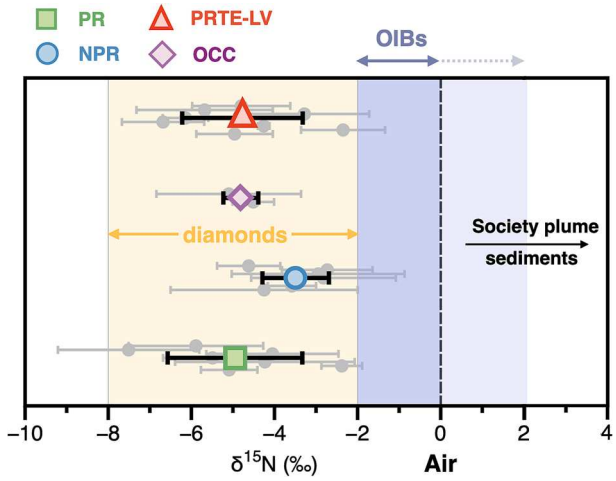

Fig. 9. Homogeneity of the N isotope composition of the upper mantle. MORB and diamond data are from this study and the compilation by Cartigny and Marty (2013), respectively. The range of N isotope compositions of −2‰ to 0 ‰ for high $^3He/^4He$ Oceanic Island Basalts (OIBs) is taken from Labidi (2022). As per this study, lavas from the Society plume with low $^3He/^4He$ ratios may be representative of an enriched mantle source, with elevated $\delta^{15}N \geq +0.5$ ‰ (Labidi, 2022). Such positive $\delta^{15}N$ are interpreted as reflecting the addition of sedimentary material with high $\delta^{15}N$ (e.g., Busigny et al., 2011) to a primitive mantle. Whether or not high $^3He/^4He$ sources may also exhibit positive $\delta^{15}N$ remains a matter of debate, which we illustrate by extending the potential range of OIB $\delta^{15}N$ with a shaded area reaching up to +2 ‰.

(e.g., Bach et al., 1994; Dosso et al., 1999; Le Roex et al., 1989; Le Roux et al., 2002; Bougault et al., 1988), requiring variable contributions from surface-derived, recycled components. Likewise, the occurrence of mantle source $^{40}Ar/^{36}Ar$ heterogeneities but homogeneous N isotope compositions further suggests that Ar and N are likely decoupled during subduction, with the main carrier phase of subducted Ar most likely being vacancies in the structure of serpentinites (e.g., Kendrick et al., 2011). The striking $\delta^{15}N$ homogeneity of MORB samples with variable K_2O/TiO_2 and mantle source $^{40}Ar/^{36}Ar$ thus appears at odds with the fact that subduction delivers sediment, altered oceanic crust, and

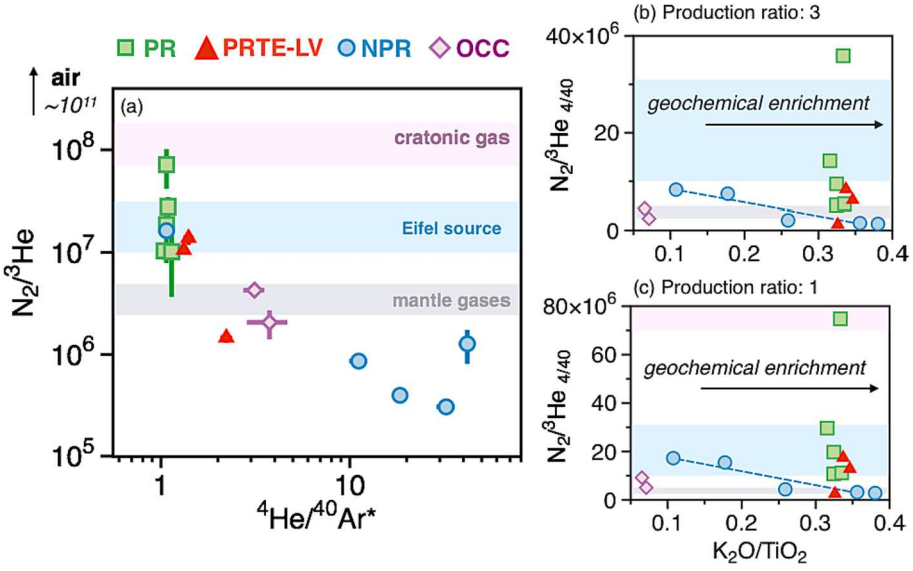

Fig. 8. $N_2/^3He$-$^4He/^{40}Ar^*$ systematics of MORB samples analyzed in this study. End-member $N_2/^3He$ compositions for cratonic gas, Eifel (Germany), and other mantle gas source compositions are from Labidi et al. (2020) and references therein. The NPR sample with a PR-like $N_2/^3He$ corresponds to NPR AL4959-406 which, despite its low vesicularity, plots within the range of popping rocks in $^4He/^{40}Ar^*$ vs. $^{40}Ar^*$ space (Bekaert et al., Part A). $N_2/^3He_{4/40}$ values, computed by assuming a $^4He/^{40}Ar^*$ mantle production ratio of 3 (b) or 1 (c), generally do not correlate with the degree of geochemical enrichment, with the potential exception of NPR samples (dashed lines with coefficients of determination of 0.88).

hydrated ultramafic rocks with generally positive $\delta^{15}N$ values arising from organic/sedimentary processes at Earth's surface (Busigny et al., 2005a; Busigny et al., 2005b; Li et al., 2007; Halama and Bebout, 2021, *and references therein*).

4.2.2.1. Bulk $\delta^{15}N$ of downgoing slabs?. While the average $\delta^{15}N$ of downgoing slabs is often considered to be ~ +6‰, reflecting dominance of sedimentary N sources, it is conceivable that the true representative slab $\delta^{15}N$ value may be closer to the canonical mantle value (~−5‰) if altered oceanic crust (rather than sediments) were to dominate the bulk N budget of typical slabs. Indeed, sediments make up only a small part of subducting plates (Plank and Langmuir, 1998; Straub and Layne, 2003; Barnes and Straub, 2010; John et al., 2011; Bekaert et al., 2021b), and it has been suggested that the nitrogen flux from subducting altered oceanic crust may actually be the dominant flux of subducting nitrogen in many regions of the globe, including the Marianas (Li et al., 2007; Mitchell et al., 2010) and New Zealand (Epstein et al., 2021). Importantly, N is introduced into the altered oceanic crust through the uptake of ammonium ions in secondary clay minerals and can be isotopically heavy (+16 ‰) or light (−12 ‰) depending if the alteration takes place at low or high temperatures, respectively (e.g., (Li et al., 2019)). Previous analyses of nitrogen in subducted altered oceanic crust or lithosphere have thus found large ranges of $\delta^{15}N$ variations (e.g., −11.6 to +8.3 ‰ (Li et al., 2007); −3.8 to 5.8 ‰ (Busigny et al., 2005b); −0.9 to +7.3 ‰ (Busigny et al., 2019)). Given the wide range of $\delta^{15}N$ signatures measured within subducting lithologies, it is difficult to determine a representative $\delta^{15}N$ for bulk subducting slabs. This may be especially true for recycled material in the mantle depending on the variable amount of nitrogen that may be retained according to the slab-specific thermal structure of any subduction zone (Mallik et al., 2018; Jackson et al., 2021) and fractionations between solid phases retained in the slab and nitrogen released in fluids (Bebout and Fogel, 1992). Thus, one cannot rule out the possibility that the $\delta^{15}N$ of slab-derived N input to the mantle is lighter than typical sedimentary N (and therefore closer to measured $\delta^{15}N$ in this and other MORB studies). Interestingly, the homogeneous $\delta^{15}N$ composition is consistent with the homogeneous light noble gas (He and Ne) isotope composition of the upper mantle, historically used as evidence for a well-mixed reservoir, potentially indicating that volatile elements (including N) are efficiently and rapidly mixed within the upper mantle, compared to non-volatile elements. To have the average $\delta^{15}N$ of bulk subducting slabs matching "by chance" the primitive composition of the upper mantle however remains unlikely, and would invariably violate independent constraints from the constant $N_2/^3He$ across MORB samples with variable K/Ti ratios (e.g., Labidi (2022)).

4.2.2.2. Chemical barriers to N subduction. Bulk N content and $\delta^{15}N$ compositions of subducting slabs are likely to be modified in a number of chemical ways during subduction. During progressive metamorphism at temperatures of ~350–550 °C (depending on pressure), devolatilization can release significant fractions of the N initially fixed in crustal rocks through organic diagenesis (Bebout et al., 2016). Challenges associated with the deconvolution of recycled and air-derived N in volcanic systems (including volcanic arcs) worldwide prevent setting unambiguous constraints on the efficiency of N recycling at subduction zones (e.g., Bekaert et al., 2023). Thus, the possibility that most of the N that is initially subducted is destabilized and quantitatively returned to the Earth's surface by degassing at the volcanic arcs cannot be discarded (Labidi and Young, 2022). Although the partitioning and overall behavior of N in slab mineral assemblages remains poorly constrained, N loss during slab dehydration could be particularly efficient along warm and oxidized subduction geotherms (Jackson et al., 2021), thereby limiting the ingassing efficiency of nitrogen to the mantle. Slab dehydration along reduced and cooler geotherms may only extract moderate amounts of nitrogen, resulting in greater ingassing efficiency of nitrogen to the deep (compared to the upper) mantle (Jackson et al., 2021). The coupling between N and other geochemical proxies for sediment input in the mantle may therefore greatly vary depending on the temperature and fO_2 conditions of a given subduction zone.

It is also worth noting that the stability of subducted N-bearing phases in the lower vs. upper mantle may also differ due to contrasting P, T, and fO_2 conditions. While N is transported to the mantle via cold slabs through NH_4 inherited from sedimentary material, and stored at high-pressure in K-bearing minerals (Halama et al., 2010; Busigny and Bebout, 2013; Cartigny and Marty, 2013), N output from the mantle happens through degassing of N_2 (Watenphul et al., 2010). The speciation (and therefore behavior) of subducting organic-sedimentary N is determined by a combination of temperature, pressure, oxygen fugacity, chemical activity, and pH, which may differ between the upper and lower mantle. Although fO_2 is the controlling factor that determines if N is molecular (N_2) or ammonic (NH_4^+ and NH_3), pH designates if ammonic nitrogen is NH_4^+ or NH_3 (Mikhail et al., 2017). The poor retention of subducted sedimentary N in the upper (compared to the lower) mantle may be due to the enhanced oxidation of NH_4 into molecular nitrogen, which is prone to loss by degassing (Watenphul et al., 2010). Conversely, the poor retention of primordial N in a given mantle reservoir could make it more prone to overprinting by subduction-derived N. The loss/preservation of primordial versus recycled N-bearing components may ultimately control the N isotope composition of the mantle and explain the striking homogeneity of N isotopes across the upper mantle (Fig. 9). The role of organic matter (stable at great depths) in delivering organic-sedimentary N to deeper mantle domains remains a promising avenue of investigation (e.g., Sadofsky and Bebout, 2004; Karleskind et al., 2011).

4.2.2.3. Physical barriers to subduction of N-rich sediments. Physical processes may prevent subducting N from reaching mantle depths. Sedimentary layers covering downgoing slabs may either be carried down to depth along the slab interface with the overriding plate, or eroded from top of the downgoing plate and appended to the accretionary wedge. The ultimate effect of sediments on subduction dynamics (and the retroactive effect of subduction dynamics on the extent of sediment accumulation within accretionary margins) is not straightforward (Behr and Becker, 2018; Brizzi et al., 2021). Nonetheless, the thickness and viscosity of subducting sediments may control the extent of frictional coupling between the plates (also known as the "lubricating effect"): higher viscous coupling favors an erosive style of margin (tectonic removal of crustal material from the overriding plate by subduction erosion), whereas reduced viscous coupling promotes accretionary wedge generation (substantial accretion of subducting plate material to the forearc owing to frontal accretion and/or underplating; Straub et al., 2020; Pusok et al., 2021). Given that the geometry of the wedge controls the bending of the slab and the radius of the curvature, it likely also determines how recycled components are introduced into the upper/lower mantle. Although tectonic erosion margins subduct a higher percentage of sediments than accretionary margins (e.g., Clift, 2017), they are typically associated with a reduced sediment cover, such that accretionary margins may ultimately subduct larger volumes of sediments (Pusok et al., 2021). We speculate that a relationship may exist between the slab dip angle/radius of curvature, the sediment flux to depths below the lithosphere, and the fate of subducted material (to the upper/lower mantle). Subduction dynamics may regulate the amount of sediments that are recycled into the mantle, and whether the absence of recycled sedimentary N in the upper mantle could be explained by the fact that shallow dip angle slabs (preferentially introduced into the upper mantle) are subject to greater sediment removal than steeply dipping slabs (preferentially introduced into the deep mantle). This could potentially contribute to explaining why positive $\delta^{15}N$ associated with sedimentary N are preferentially observed in the deep (and not the upper) mantle (Marty and Dauphas, 2003; Barry and Hilton, 2016; Bekaert et al., 2021b).

Most conceptual models assume that sediments are – at least partially – transported to depth with the subducting plate. However, numerical and analog modeling studies indicate that buoyant material, including sediments, may separate from the subducting plate at shallow depths (e.g., Gerya and Yuen, 2003; Boutelier et al., 2004). Owing to their low density relative to the mantle, sediments are expected to detach from the subducting plate at ~100 km depth, for a wide range of sediment densities and rheologies (Currie et al., 2007). Sediment detachment may vastly reduce sediment transport to the mantle, in particular for regions where the subducted sediment thickness is $\geq$ ~350 m (Currie et al., 2007). The physical separation of sediments and oceanic crust during subduction may contribute to explaining the absence of sedimentary N and widespread occurrence of recycled oceanic crust across the upper mantle.

4.2.2.4. Fingerprints from Earth's accretion/differentiation?. The $N_2/^3He$ and $\delta^{15}N$ characteristics of Earth's mantle may have been established during terrestrial formation and early evolution (Labidi, 2022). Interestingly, however, many planetary processes potentially modified the N isotope composition of the solid Earth, and potentially introduced planetary N isotope variations that are no longer present in the modern day mantle. For instance, Earth is considered to have inherited its volatile budget from the heterogeneous accretion of planetary bodies originating from various heliocentric distances in the Solar System (Broadley et al., 2022). However, the planetary precursors of terrestrial accretion likely exhibited a great variability of N isotope compositions, including enstatite ($\delta^{15}N$ in the range −40 to ~0 ‰) and carbonaceous ($\delta^{15}N$ in the range ~0 to +60 ‰) chondrite-like materials (Piani et al., 2020), differentiated planetary bodies (Grewal et al., 2021) and comets (Jehin et al., 2009). The uniform N isotope composition of the upper mantle therefore requires efficient mixing and homogenization of its initial budget, which could have been achieved during the magma ocean stage. Notably, the observed $\delta^{15}N$ disequilibrium between the MORB mantle and the atmosphere could be mostly accounted for by magma ocean degassing under low fO_2 (e.g., Labidi (2022)). It is also noteworthy that some extent of N isotope fractionation (Dalou et al., 2019; Li et al., 2016) during partitioning into Earth's core (e.g., Johnson and Goldblatt, 2015) could have contributed to introducing N isotope differences between different reservoirs of the solid Earth. These distinct processes could explain the present-day distribution and composition of N in terrestrial reservoirs, without requiring significant N exchange via subduction.

5. Conclusions

Mid-ocean ridges provide a direct window into the heterogeneous nature of the upper mantle, whose geochemical composition can be probed to decipher the long-term evolution of our planet. In this study, we combine the isotopic analysis of volatile (carbon, nitrogen, noble gases) and radiogenic (Pb, Sr, Nd) elements, as well as the abundances of major and trace elements, to document the origin of upper mantle geochemical heterogeneities near 14°N on the Mid-Atlantic Ridge. These data unequivocally show that the mantle source of OCC samples (which we classify as a "young" HIMU-influenced N-MORB) is distinct from the mantle source of geochemically enriched, PR-affiliated samples (E-MORBs). Taken together, our data do not support the existence of a ridge-centered, primitive mantle plume near 14°N on the MAR (e.g., Dosso et al., 1991; Bougault et al., 1988; Long et al., 2019) nor significant contribution of recycled sediments in the mantle source, therefore calling for alternative processes to account for the observed mantle source heterogeneities. Possible scenarios may include contribution from old, subducted crust (devoid of sediments; Staudacher et al., 1989) or relics of sub-continental lithospheric mantle removed from the continents during continental break-up (Bonatti et al., 1992; Dosso et al., 1999; Hoernle et al., 2011). Regardless, the observation of mantle source geochemical heterogeneities at the local scale (i.e., near 14°N on the MAR) appears consistent with the occurrence of dispersed, recycled crustal components across the upper mantle (Stracke, 2012), as proposed in the framework of the "marble-cake" mantle (Allègre and Turcotte, 1986).

In this paper, we also focus on the remarkable absence of significant $\delta^{15}N$ variation across N-MORB and E-MORB samples (average $\delta^{15}N = -4.49 \pm 1.40$ ‰ in this study). The extent to which the surmised N isotope variability of planetary precursors of terrestrial accretion was homogenized, and uniformly affected by fractionation processes (e.g., during partitioning into Earth's core), remains poorly understood. Overall, the possibility that the average $\delta^{15}N$ of bulk subducting slabs matches "by chance" the primitive composition of the upper mantle is unlikely, as it would invariably violate independent constraints from the constant $N_2/^3He$ across MORB samples with variable K/Ti ratios. Therefore, we envision a series of chemical and physical processes that may contribute to reducing the contribution of recycled sedimentary nitrogen to the overall budget of the upper mantle. This may involve specific P, T, and fO_2 conditions during subduction and storage within the mantle, as well as slab dip angle-controlled physical separation of sediments and oceanic crust upon subduction. These considerations however remain fairly speculative, and call for more experimental and theoretical work to disentangle the relative contributions of primordial (terrestrial accretion and differentiation) and secondary (subduction) processes in producing the N isotope characteristics of the solid Earth.

Declaration of competing interest

The authors declare that they have no known competing financial interests or personal relationships that could have appeared to influence the work reported in this paper.

Data availability

Data are available through Zenodo at: https://zenodo.org/records/10033391.

Acknowledgements

We gratefully acknowledge the Captain, operations teams, marine technicians, and crew of the *R/V Atlantis*, the operations teams of the *AUV Sentry*and *HOV Alvin*, and the entire scientific party on-board AT33-03 and AT40-02 expeditions. We thank Al Gagnon at NOSAMS for assistance with the carbon isotope measurements, as well as Max Jones for constructive discussions. We thank Max Jones for constructive discussions. We thank Phillipe Sarda, Pierre Cartigny, and two anonymous reviewers for detailed and constructive reviews, as well as Manuel Moreira for careful editorial oversight. Seagoing and analytical efforts were supported by National Science Foundation (NSF) grants OCE-1259218, OCE-1260578, and MGG-2015789 to M. Kurz, E. Mittelstaedt, and P. Barry, respectively.

Appendix A. Supplementary material

Supplementary material includes a neon three-isotope plot of MORB samples analyzed in this study. Supplementary material to this article can be found online at https://doi.org/10.1016/j.gca.2023.12.017.

References

Abouchami, W., Galer, S.J.G., Koschinsky, A., 1999. Abouchami-1999-Pb and Nd isotopes in NE Atlant.pdf. Geochim. Cosmochim. Acta 63, 1489–1505.
Abouchami, W., Galer, S.J.G., Hofmann, A.W., 2000. High precision lead isotope systematics of lavas from the Hawaiian Scientific Drilling Project. Chem. Geol. 169, 187–209.

Allègre, C.J., Hamelin, B., Dupré, B., 1984. Statistical analysis of isotopic ratios in MORB: the mantle blob cluster model and the convective regime of the mantle. Earth Planet. Sci. Lett. 71 (1), 71–84.
Allègre, C.J., Turcotte, D.L., 1986. Implications of a two-component marble-cake mantle. Nature 323, 123–127.
Anderson, D.L., 2006. Speculations on the nature and cause of mantle heterogeneity. Tectonophysics 416 (1–4), 7–22.
Bach, W., Hegner, E., Erzinger, J., Satir, M., 1994. Chemical and isotopic variations along the superfast spreading East Pacific Rise from 6 to 30 S. Contrib. Mineral. Petrol. 116, 365–380.
Barfod, D.N., Ballentine, C.J., Halliday, A.N., Fitton, J.G., 1999. Noble gases in the Cameroon line and the He, Ne, and Ar isotopic compositions of high (HIMU) mantle. J. Geophys. Res. 104 (B12), 29509–29527.
Barnes, J.D., Straub, S.M., 2010. Chorine stable isotope variations in Izu Bonin tephra: implications for serpentinite subduction. Chem. Geol. 272, 62–74.
Barry, P.H., Hilton, D.R., 2016. Release of subducted sedimentary nitrogen throughout Earth's mantle. Geochem. Perspectives Lett. 2, 148–159.
Bebout, G.E., Fogel, M.L., 1992. Nitrogen-isotope compositions of metasedimentary rocks in the Catalina Schist, California: implications for metamorphic devolatilization history. Geochim. Cosmochim. Acta 56 (7), 2839–2849.
Bebout, G.E., Lazzeri, K.E., Geiger, C.A., 2016. Pathways for nitrogen cycling in Earth's crust and upper mantle: A review and new results for microporous beryl and cordierite. Am. Min. 101 (1), 7–24.
Behr, W.M., Becker, T.W., 2018. Sediment control on subduction plate speeds. Earth Planet. Sci. Lett. 502, 166–173.
Bekaert, D.V., et al., 2021a. High 3He/4He in central Panama reveals a distal connection to the Galápagos plume. Proc. Natl. Acad. Sci. 118 (47), e2110997118.
Bekaert, D.V., Turner, S.J., Broadley, M.W., Barnes, J.D., Halldoacutersson, S.A., Labidi, J., Wade, J., Walowski, K.J., Barry, P.H., 2021b. Subduction-driven volatile recycling: a global mass balance. Annu. Rev. Earth Planet. Sci. 49, 37–70.
Bekaert, D.V., Barry, P.H., Broadley, M.W., Byrne, D.J., Marty, B., Ramírez, C.J., Seltzer, A.M., 2023. Ultrahigh-precision noble gas isotope analyses reveal pervasive subsurface fractionation in hydrothermal systems. Sci. Adv. 9 (15), eadg2566.
Bergin, E.A., Blake, G.A., Ciesla, F., Hirschmann, M.M., Li, J., 2015. Tracing the ingredients for a habitable earth from interstellar space through planet formation. Proc. Natl. Acad. Sci. U.S.A. 112, 8965–8970.
Bonatti, E., Peyve, A., Kepezhinskas, P., Kurentsova, N., Seyler, M., Skolotnev, S., Udintsev, G., 1992. Upper mantle heterogeneity below the Mid-Atlantic Ridge, 0°-15°N. J. Geophys. Res. 97, 4461–4476.
Bougault, H., Dmitriev, L., Schilling, J.G., Sobolev, A., Joron, J.L., Needham, H.D., 1988. Mantle heterogeneity from trace elements: MAR triple junction near 14°N. Earth Planet. Sci. Lett. 88, 27–36.
Boutelier, D., Chemenda, A., Jorand, C., 2004. Continental subduction and exhumation of high-pressure rocks: Insights from thermo-mechanical laboratory modelling. Earth Planet. Sci. Lett. 222, 209–216.
Brizzi, S., Becker, T.W., Faccenna, C., Behr, W., van Zelst, I., Dal Zilio, L., van Dinther, Y., 2021. The role of sediment accretion and buoyancy on subduction dynamics and geometry. Geophys. Res. Lett. 48, 1–12.
Broadley, M.W., Barry, P.H., Bekaert, D.V., Byrne, D.J., Caracausi, A., Ballentine, C.J., Marty, B., 2020. Identification of chondritic krypton and xenon in Yellowstone gases and the timing of terrestrial volatile accretion. Proc. Natl. Acad. Sci. U.S.A. 117, 13997–14004.
Broadley, M.W., Bekaert, D.V., Piani, L., Füri, E., Marty, B., 2022. Origin of life-forming volatile elements in the inner Solar System. Nature 611 (7935), 245–255.
Busigny, V., Ader, M., Cartigny, P., 2005a. Quantification and isotopic analysis of nitrogen in rocks at the ppm level using sealed tube combustion technique: a prelude to the study of altered oceanic crust. Chem. Geol. 223, 249–258.
Busigny, V., Bebout, G.E., 2013. Nitrogen in the silicate earth: speciation and isotopic behavior during mineral-fluid interactions. Elements 9, 353–358.
Busigny, V., Laverne, C., Bonifacie, M., 2005b. Nitrogen content and isotopic composition of oceanic crust at a superfast spreading ridge: a profile in altered basalts from ODP Site 1256, Leg 206. Geochem. Geophys. Geosyst. 6 (12).
Busigny, V., Cartigny, P., Philippot, P., 2011. Nitrogen isotopes in ophiolitic metagabbros: a re-evaluation of modern nitrogen fluxes in subduction zones and implication for the early Earth atmosphere. Geochim. Cosmochim. Acta 75, 7502–7521.
Busigny, V., Cartigny, P., Laverne, C., Teagle, D., Bonifacie, M., Agrinier, P., 2019. A re-assessment of the nitrogen geochemical behavior in upper oceanic crust from Hole 504B: implications for subduction budget in Central America. Earth Planet. Sci. Lett. 525, 115735.
Cartigny, P., Marty, B., 2013. Nitrogen isotopes and mantle geodynamics: the emergence of life and the atmosphere-crust-mantle connection. Elements 9, 359–366.
Cartigny, P., Jendrzejewski, N., Pineau, F., Petit, E., Javoy, M., 2001. Volatile (C, N, Ar) variability in MORB and the respective roles of mantle source heterogeneity and degassing: the case of the Southwest Indian Ridge. Earth Planet. Sci. Lett. 194, 241–257.
Cartigny, P., Pineau, F., Aubaud, C., Javoy, M., 2008. Towards a consistent mantle carbon flux estimate: Insights from volatile systematics (H_2O/Ce, δD, CO_2/Nb) in the North Atlantic mantle (14° N and 34° N). Earth Planet. Sci. Lett. 265, 672–685.
Chauvel, C., Hofmann, A.W., Vidal, P., 1992. HIMU-EM: the French Polynesian connection. Earth Planet. Sci. Lett. 110 (1–4), 99–119.
Clarke, W.B., Jenkins, W.J., Top, Z., 1976. Determination of tritium by mass spectrometric measurement of ^{3}He. Int. J. Appl. Radiat. Isot. 27 (9), 515–522.
Clift, P.D., 2017. A revised budget for Cenozoic sedimentary carbon subduction. Rev. Geophys. 55, 97–125.
Colin, A., Burnard, P.G., Graham, D.W., Marrocchi, Y., 2011. Plume–ridge interaction along the Galapagos Spreading Center: discerning between gas loss and source effects using neon isotopic compositions and ^{4}He–^{40}Ar*–CO_2 relative abundances. Geochim. Cosmochim. Acta 75 (4), 1145–1160.
Currie, C.A., Beaumont, C., Huismans, R.S., 2007. The fate of subducted sediments: a case for backarc intrusion and underplating. Geology 35 (2), 1111–1114.
Dalou, C., Hirschmann, M.M., von der Handt, A., Mosenfelder, J., Armstrong, L.S., 2017. Nitrogen and carbon fractionation during core–mantle differentiation at shallow depth. Earth Planet. Sci. Lett. 458, 141–151.
Dalou, C., Füri, E., Deligny, C., Piani, L., Caumon, M.C., Laumonier, M., Boulliung, J., Edén, M., 2019. Redox control on nitrogen isotope fractionation during planetary core formation. Proc. Natl. Acad. Sci. U.S.A. 116, 14485–14494.
Day, J.M.D., Hilton, D.R., 2011. Origin of ^{3}He/^{4}He ratios in HIMU-type basalts constrained from Canary Island lavas. Earth Planet. Sci. Lett. 305, 226–234.
Donnelly, K.E., Goldstein, S.L., Langmuir, C.H., Spiegelman, M., 2004. Origin of enriched ocean ridge basalts and implications for mantle dynamics. Earth Planet. Sci. Lett. 226, 347–366.
Dosso, L., Hanan, B.B., Bougault, H., Schilling, J.G., Joron, J.L., 1991. Sr-Nd-Pb geochemical morphology between 10° and 17°N on the Mid-Atlantic Ridge: a new MORB isotope signature. Earth Planet. Sci. Lett. 106, 29–43.
Dosso, L., Bougault, H., Langmuir, C., Bollinger, C., Bonnier, O., Etoubleau, J., 1999. The age and distribution of mantle heterogeneity along the Mid-Atlantic ridge (31–41°N). Earth Planet. Sci. Lett. 170, 269–286.
Epstein, G.S., Bebout, G.E., Christenson, B.W., Sumino, H., Wada, I., Werner, C., Hilton, D.R., 2021. Cycling of CO_2 and N_2 along the Hikurangi Subduction Margin, New Zealand: An integrated geological, theoretical, and isotopic approach. Geochem. Geophys. Geosyst. 22 (9), e2021GC009650.
Georgen, J.E., Kurz, M.D., Dick, H.J.B., Lin, J., 2003. Low 3He/4He ratios in basalt glasses from the western Southwest Indian Ridge (10°-24°E). Earth Planet. Sci. Lett. 206, 509–528.
Gerya, T.V., Yuen, D.A., 2003. Rayleigh - Taylor instabilities from hydration and melting propel "cold plumes" at subduction zones. Earth Planet. Sci. Lett. 212, 47–62.
Graham, D.W., 2002. Noble gas isotope geochemistry of mid-ocean ridge and ocean island basalts: Characterization of mantle source reservoirs. Rev. Mineral. Geochem. 47 (1), 247–317.
Graham, D.W., Michael, P.J., 2021. Predominantly recycled carbon in Earth's upper mantle revealed by He-CO_2-Ba systematics in ultradepleted ocean ridge basalts. Earth Planet. Sci. Lett. 554, 116646.
Graham, D.W., Lupton, J.E., Spera, F.J., Christie, D.M., 2001. Upper-mantle dynamics revealed by helium isotope variations along the southeast indian ridge. Nature 409, 701–703.
Graham, D.W., Hanan, B.B., Hémond, C., Blichert-toft, J., Albarède, F., 2014. Helium isotopic textures in Earth's upper mantle. Geochem. Geophys. Geosyst. 15 (5), 2048–2074.
Grewal, D.S., Dasgupta, R., Farnell, A., 2020. The speciation of carbon, nitrogen, and water in magma oceans and its effect on volatile partitioning between major reservoirs of the Solar System rocky bodies. Geochim. Cosmochim. Acta 280, 281–301.
Grewal, D.S., Dasgupta, R., Marty, B., 2021. A very early origin of isotopically distinct nitrogen in inner Solar System protoplanets. Nat. Astron 5, 356–364.
Halama, R., Bebout, G., 2021. Earth's nitrogen and carbon cycles. Space Sci. Rev. 217 (3), 45.
Halama, R., Bebout, G.E., John, T., Schenk, V., 2010. Nitrogen recycling in subducted oceanic lithosphere: The record in high- and ultrahigh-pressure metabasaltic rocks. Geochim. Cosmochim. Acta 74, 1636–1652.
Halldórsson, S.A., Hilton, D.R., Barry, P.H., Füri, E., Grönvold, K., 2016. Recycling of crustal material by the Iceland mantle plume: new evidence from nitrogen elemental and isotope systematics of subglacial basalts. Geochim. Cosmochim. Acta 176, 206–226.
Hanyu, T., Kaneoka, I., 1997. The uniformand low 3He/4He ratios of HIMU basalts as evidence for their origin as recycled materials. Nature 390, 273–276.
Hanyu, T., Tatsumi, Y., Kimura, J.I., 2011. Constraints on the origin of the HIMU reservoir from He-Ne-Ar isotope systematics. Earth Planet. Sci. Lett. 307, 377–386.
Hart, S.R., 1984. The DUPAL anomaly: A large-scale isotopic anomaly in the southern hemisphere. Nature 309, 753–756.
Hart, S.R., Blusztajn, J., 2006. Age and geochemistry of the mafic sills, ODP site 1276, Newfoundland margin. Chem. Geol. 235, 222–237.
Hart, S.R., Coetzee, M., Workman, R.K., Blusztajn, J., Johnson, K.T.M., Sinton, J.M., Steinberger, B., Hawkins, J.W., 2004. Genesis of the Western Samoa seamount province: age, geochemical fingerprint and tectonics. Earth Planet. Sci. Lett. 227, 37–56.
Hirschmann, M.M., 2018. Comparative deep Earth volatile cycles: The case for C recycling from exosphere/mantle fractionation of major (H_2O, C, N) volatiles and from H_2O/Ce, CO_2/Ba, and CO_2/Nb exosphere ratios. Earth Planet. Sci. Lett. 502, 262–273.
Hoernle, K., Hauff, F., Werner, R., Van Den Bogaard, P., Gibbons, A.D., Conrad, S., Müller, R.D., 2011. Origin of Indian Ocean Seamount Province by shallow recycling of continental lithosphere. Nat. Geosci. 4, 883–887.
Hofmann, A.W., 2007. Sampling mantle heterogeneity through oceanic basalts: isotopes and trace elements. Treatise Geochem. 2, 568.
Holland, G., Ballentine, C.J., 2006. Seawater subduction controls the heavy noble gas composition of the mantle. Nature 441, 186–191.
Jackson, C.R.M., Cottrell, E., Andrews, B., 2021. Warm and oxidizing slabs limit ingassing efficiency of nitrogen to the mantle. Earth Planet. Sci. Lett. 553, 116615.

Jackson, M.G., Hart, S.R., 2006. Strontium isotopes in melt inclusions from Samoan basalts: implications for heterogeneity in the Samoan plume. Earth Planet. Sci. Lett. 245, 260–277.
Jackson, M.G., Hart, S.R., Koppers, A.A.P., Staudigel, H., Konter, J., Blusztajn, J., Kurz, M., Russell, J.A., 2007. The return of subducted continental crust in Samoan lavas. Nature 448, 684–687.
Javoy, M., Pineau, F., 1991. The volatiles record of a "popping" rock from the Mid-Atlantic Ridge at 14 ° N: chemical and isotopic composition of gas trapped in the vesicles. Earth Planet. Sci. Lett. 107, 598–611.
Jehin, E., Manfroid, J., Hutsemékers, D., Arpigny, C., Zucconi, J.M., 2009. Isotopic ratios in comets: status and perspectives. Earth Moon Planet. 105, 167–180.
John, T., Scambelluri, M., Frische, M., Barnes, J.D., Bach, W., 2011. Dehydration of subducting serpentinite: implications for halogen mobility in subduction zones and the deep halogen cycle. Earth Planet. Sci. Lett. 308, 65–76.
Johnson, B., Goldblatt, C., 2015. The nitrogen budget of Earth. Earth Sci. Rev. 148, 150–173.
Jones, M.R., et al., 2019. New constraints on mantle carbon from Mid-Atlantic Ridge popping rocks. Earth Planet. Sci. Lett. 511, 67–75.
Karleskind, P., Lévy, M., Memery, L., 2011. Subduction of carbon, nitrogen, and oxygen in the northeast Atlantic. J. Geophys. Res. Oceans 116, 1–17.
Kendrick, M.A., Scambelluri, M., Honda, M., Phillips, D., 2011. High abundances of noble gas and chlorine delivered to the mantle by serpentinite subduction. Nat. Geosci. 4, 807–812.
Kendrick, M.A., Scambelluri, M., Hermann, J., Padrón-Navarta, J.A., 2018. Halogens and noble gases in serpentinites and secondary peridotites: Implications for seawater subduction and the origin of mantle neon. Geochim. Cosmochim. Acta 235, 285–304.
Kienast, M., 2000. Unchanged nitrogen isotopic composition of organic matter in the South China Sea during the last climatic cycle: global implications. Paleoceanography 15 (2), 244–253.
Klein, E.M., Langmuir, C.H., 1987. Global correlations of ocean ridge basalt chemistry with axial depth and crustal thickness. J. Geophys. Res. Solid Earth 92 (B8), 8089–8115.
Koppers, A.A., Becker, T.W., Jackson, M.G., Konrad, K., Müller, R.D., Romanowicz, B., Whittaker, J.M., 2021. Mantle plumes and their role in Earth processes. Nat. Rev. Earth Environ. 2 (6), 382–401.
Kurz, M.D., Jenkins, W.J., Schilling, J.G., Hart, S.R., 1982. Helium isotopic variations in the mantle beneath the central North Atlantic Ocean. Earth Planet. Sci. Lett. 58, 1–14.
Kurz, M.D., Moreira, M., Curtice, J., Lott, D.E., Mahoney, J.J., Sinton, J.M., 2005. Correlated helium, neon, and melt production on the super-fast spreading East Pacific Rise near 17°S. Earth Planet. Sci. Lett. 232, 125–142.
Labidi, J., et al., 2020. Hydrothermal $^{15}N^{15}N$ abundances constrain the origins of mantle nitrogen. Nature 580, 367–371.
Labidi, J., 2022. The origin of nitrogen in Earth's mantle: Constraints from basalts $^{15}N/^{14}N$ and $N_2/^3He$ ratios. Chem. Geol. 597, 120780.
Labidi, J., Young, E.D., 2022. The origin and dynamics of nitrogen in the Earth's mantle constrained by $^{15}N^{15}N$ in hydrothermal gases. Chem. Geol. 591, 120709.
Le Roex, Dick, H.J., Fisher, R.L., 1989. Petrology and geochemistry of MORB from 25 E to 46 E along the Southwest Indian Ridge: evidence for contrasting styles of mantle enrichment. J. Petrol. 30 (4), 947–986.
Le Roux, Le Roex, Schilling, J.G., Shimizu, N., Perkins, W.W., Pearce, N.J.G., 2002. Mantle heterogeneity beneath the southern Mid-Atlantic Ridge: trace element evidence for contamination of ambient asthenospheric mantle. Earth Planet. Sci. Lett. 203 (1), 479–498.
Le Voyer, M., Hauri, E.H., Cottrell, E., Kelley, K.A., Salters, V.J.M., Langmuir, C.H., Hilton, D.R., Barry, P.H., Füri, E., 2019. Carbon fluxes and primary magma CO_2 contents along the global mid-ocean ridge system. Geochem. Geophys. Geosyst. 20, 1387–1424.
Li, L., Bebout, G.E., Idleman, B.D., 2007. Nitrogen concentration and $\delta^{15}N$ of altered oceanic crust obtained on ODP Legs 129 and 185: Insights into alteration-related nitrogen enrichment and the nitrogen subduction budget. Geochim. Cosmochim. Acta 71, 2344–2360.
Li, K., Li, L., Pearson, D.G., Stachel, T., 2019. Diamond isotope compositions indicate altered igneous oceanic crust dominates deep carbon recycling. Earth Planet. Sci. Lett. 516, 190–201.
Li, Y.F., Marty, B., Shcheka, S., Zimmermann, L., Keppler, H., 2016. Nitrogen isotope fractionation during terrestrial core-mantle separation. Geochem. Perspectives Lett. 2, 138–147.
Liu, B., Liang, Y., 2017. The prevalence of kilometer-scale heterogeneity in the source region of MORB upper mantle. Sci. Adv. 3 (11), e1701872.
Long, X., Geldmacher, J., Hoernle, K., Hauff, F., Wartho, J., Garbe-schönberg, D., Grevemeyer, I., 2019. Age and origin of Researcher Ridge and an explanation for the 14°N anomaly on the Mid-Atlantic Ridge by plume-ridge interaction. Lithos 326, 540–555.
Mallik, A., Li, Y., Wiedenbeck, M., 2018. Nitrogen evolution within the Earth's atmosphere–mantle system assessed by recycling in subduction zones. Earth Planet. Sci. Lett. 482, 556–566.
Marty, B., 2012. The origins and concentrations of water, carbon, nitrogen and noble gases on Earth. Earth Planet. Sci. Lett. 313–314, 56–66.
Marty, B., Almayrac, M., Barry, P.H., Bekaert, D.V., Broadley, M.W., Byrne, D.J., Ballentine, C.J., Caracausi, A., 2020. An evaluation of the C/N ratio of the mantle from natural CO_2-rich gas analysis: geochemical and cosmochemical implications. Earth Planet. Sci. Lett. 551, 116574.
Marty, B., Dauphas, N., 2003. The nitrogen record for crust-mantle interaction and mantle convection from Archean to Present. Earth Planet. Sci. Lett. 206, 397–410.
Marty, B., Humbert, F., 1997. Nitrogen and argon isotopes in oceanic basalts. Earth Planet. Sci. Lett. 152, 101–112.
Marty, B., Zimmermann, L., 1999. Volatiles (He, C, N, Ar) in mid-ocean ridge basalts: assesment of shallow-level fractionation and characterization of source composition. Geochim. Cosmochim. Acta 63, 3619–3633.
Meyzen, C.M., Blichert-Toft, J., Ludden, J.N., Humler, E., Mével, C., Albarède, F., 2007. Isotopic portrayal of the Earth's upper mantle flow field. Nature 447, 1069–1074.
Mikhail, S., Barry, P.H., Sverjensky, D.A., 2017. The relationship between mantle pH and the deep nitrogen cycle. Geochim. Cosmochim. Acta 209, 149–160.
Mitchell, E.C., Fischer, T.P., Hilton, D.R., Hauri, E.H., Shaw, A.M., de Moor, J.M., Kazahaya, K., 2010. Nitrogen sources and recycling at subduction zones: insights from the Izu-Bonin-Mariana arc. Geochem. Geophys. Geosyst. 11 (2).
Moreira, M., Kunz, J., Allegre, C., 1998. Rare gas systematics in popping rock: isotopic and elemental compositions in the Upper Mantle. Science 279 (5354), 1178–1181.
Moreira, M., Kurz, M.D., 2001. Subducted oceanic lithosphere and the origin of the "high μ" basalt helium isotopic signature. Earth Planet. Sci. Lett. 189, 49–57.
Mukhopadhyay, S., 2012. Early differentiation and volatile accretion recorded in deep-mantle neon and xenon. Nature 486, 101–104.
Mundl-Petermeier, A., Walker, R.J., Fischer, R.A., Lekic, V., Jackson, M.G., Kurz, M.D., 2020. Anomalous ^{182}W in high $^3He/^4He$ ocean island basalts: fingerprints of Earth's core? Geochim. Cosmochim. Acta 271, 194–211.
Nishio, Y., Ishii, T., Gamo, T., Sano, Y., 1999. Volatile element isotopic systematics of the Rodrigues Triple Junction Indian Ocean MORB: implications for mantle heterogeneity. Earth Planet. Sci. Lett. 170 (3), 241–253.
Parai, R., Mukhopadhyay, S., 2021. Heavy noble gas signatures of the North Atlantic Popping Rock 2ΠD43: Implications for mantle noble gas heterogeneity. Geochim. Cosmochim. Acta 294, 89–105.
Parai, R., Mukhopadhyay, S., Standish, J.J., 2012. Heterogeneous upper mantle Ne, Ar and Xe isotopic compositions and a possible Dupal noble gas signature recorded in basalts from the Southwest Indian Ridge. Earth Planet. Sci. Lett. 359–360, 227–239.
Parnell-Turner, R.E., Mittelstaedt, E., Kurz, M.D., Jones, M.R., Soule, S.A., Klein, F., Wanless, V.D., Fornari, D.J., 2018. The final stages of slip and volcanism on an oceanic detachment fault at 13°48′N, Mid-Atlantic Ridge. Geochem. Geophys. Geosyst. 19, 3115–3127.
Péron, S., et al., 2019. Noble gas systematics in new popping rocks from the Mid-Atlantic Ridge (14°N): Evidence for small-scale upper mantle heterogeneities. Earth Planet. Sci. Lett. 519, 70–82.
Peters, K.E., Sweeney, R.E., Kaplan, I.R., 1978. Correlation of carbon and nitrogen stable isotope ratios in sedimentary organic matter. Limnol. Oceanography 23, 598–604.
Piani, L., Marrocchi, Y., Rigaudier, T., Vacher, L.G., Thomassin, D., Marty, B., 2020. Earth's water may have been inherited from material similar to enstatite chondrite meteorites. Science 369, 1110–1113.
Plank, T., Langmuir, C.H., 1998. The chemical composition of subducting sediment and its consequences for the crust and mantle. Chem. Geol. 145, 325–394.
Porcelli, D., Wasserburg, G.J., 1995. Mass transfer of helium, neon, argon, and xenon through a steady-state upper mantle. Geochim. Cosmochim. Acta 59, 4921–4937.
Poreda, R., Craig, H., 1989. Helium isotope ratios in circum-Pacific volcanic arcs. Nature 338, 473–478.
Pusok, A.E., Stegman, D.R., Kerr, M., 2021. The effect of sediments on the dynamics and accretionary style of subduction margins. Solid Earth 2021, 1–30.
Roskosz, M., Bouhifd, M.A., Jephcoat, A.P., Marty, B., Mysen, B.O., 2013. Nitrogen solubility in molten metal and silicate at high pressure and temperature. Geochim. Cosmochim. Acta 121, 15–28.
Sadofsky, S.J., Bebout, G.E., 2004. Nitrogen geochemistry of subducting sediments: New results from the Izu-Bonin-Mariana margin and insights regarding global nitrogen subduction. Geochem. Geophys. Geosyst. 5, 1–23.
Sano, Y., Takahata, N., Nishio, Y., Marty, B., 1998. Nitrogen recycling in subduction zones. Geophys. Res. Lett. 25 (13), 2289–2292.
Sarda, P., Moreira, M., Staudacher, T., 1999. Argon-lead isotopic correlation in Mid-Atlantic Ridge basalts. Science 283, 666–668.
Schilling, J., Hanan, B.B., Mccully, B., Kingsley, R.H., 1994. Mantle heterogeneity from trace elements: MAR triple junction near 14°N. Earth Planet. Sci. Lett. 99, 5–12.
Shirey, S.B., Richardson, S.H., 2011. Start of the wilson cycle at 3 Ga shown by diamonds from subcontinental mantle. Science 333, 434–436.
Sleep, N.H., 1996. Lateral flow of hot plume material ponded at sublithospheric depths. J. Geophys. Res. B: Solid Earth 101, 28065–28083.
Smit, K.V., Shirey, S.B., Hauri, E.H., Stern, R.A., 2019. Sulfur isotopes in diamonds reveal differences in continent construction. Science 364, 383–385.
Staudacher, T., Allègre, C.J., 1988. Recycling of oceanic crust and sediments: the noble gas subduction barrier. Earth Planet. Sci. Lett. 89 (2), 173–183.
Staudacher, T., Sarda, P., Richardson, S.H., Allègre, C.J., Sagna, I., Dmitriev, L.V., 1989. Noble gases in basalt glasses from a Mid-Atlantic Ridge topographic high at 14°N: geodynamic consequences. Earth Planet. Sci. Lett. 96, 119–133.
Stracke, A., 2012. Earth's heterogeneous mantle: A product of convection-driven interaction between crust and mantle. Chem. Geol. 330–331, 274–299.
Straub, S.M., Gómez-Tuena, A., Vannucchi, P., 2020. Subduction erosion and arc volcanism. Nat. Rev. Earth Environ. 1, 574–589.
Straub, S.M., Layne, G.D., 2003. The systematics of chlorine, fluorine, and water in Izu arc front volcanic rocks: implications for volatile recycling in subduction zones. Geochim. Cosmochim. Acta 67, 4179–4203.
Sun, S.S., McDonough, W.F., 1989. Chemical and isotopic systematics of oceanic basalts: implications for mantle composition and processes. Geochem. Soc. Spec. Publ. 42, 313–345.
Tanaka, T., et al., 2000. JNdi-1: a neodymium isotopic reference in consistency with LaJolla neodymium. Chem. Geol. 168, 279–281.

Thirlwall, M.F., 1997. Pb isotopic and elemental evidence for OIB derivation from young HIMU mantle. Chem. Geol. 139 (1–4), 51–74.
Todt, W., Cliff, R.A., Hofmann, A.W., 1996. Evaluation of a ^{202}Pb-^{205}Pb double spike for high-precision lead isotope analysis. Earth Processes: Reading the Isotopic Code 95, 429.
Tucker, J.M., Mukhopadhyay, S., Schilling, J.G., 2012. The heavy noble gas composition of the depleted MORB mantle (DMM) and its implications for the preservation of heterogeneities in the mantle. Earth Planet. Sci. Lett. 355–356, 244–254.
Tucker, J.M., Mukhopadhyay, S., Gonnermann, H.M., 2018. Reconstructing mantle carbon and noble gas contents from degassed mid-ocean ridge basalts. Earth Planet. Sci. Lett. 496, 108–119.
Tucker, J.M., van Keken, P.E., Ballentine, C.J., 2022. Earth's missing argon paradox resolved by recycling of oceanic crust. Nat. Geosci. 15, 85–90.
Ulrich, M., Hémond, C., Nonnotte, P., Jochum, K.P., 2012. OIB/seamount recycling as a possible process for E-MORB genesis. Geochem. Geophys. Geosyst. 13, 1–24.
Watenphul, A., Wunder, B., Wirth, R., Heinrich, W., 2010. Ammonium-bearing clinopyroxene: A potential nitrogen reservoir in the Earth's mantle. Chem. Geol. 270, 240–248.
Weis, D., et al., 2006. High-precision isotopic characterization of USGS reference materials by TIMS and MC-ICP-MS. Geochem. Geophys. Geosyst. 7 (8).
White, W.M., Patchett, J., 1984. HfNdSr isotopes and incompatible element abundances in island arcs: implications for magma origins and crust-mantle evolution. Earth Planet. Sci. Lett. 67, 167–185.
Zindler, A., Hart, S., 1986. Chemical geodynamics. Annu. Rev. Earth Planet. Sci. 14 (1), 493–571.